Spectral Stability of Plasma Flows In the Magnetic Nozzle

Hunt Feng

July 2, 2024

Contents

Abstract

In this thesis, spectral stability of plasmas is understood as an eigenvalue problem of linearized plasma equations describing time dynamics near some equilibrium state. Presence of eigenvalues with positive imaginary part would indicate the instability when small fluctuations will grow (typically exponentially) in time. A particular focus is the stability of plasma with stationary flows, in particular, flows in the magnetic nozzle. Magnetic nozzle, or magnetic mirror configurations, with converging-diverging magnetic field are used to accelerate plasma in plasma propulsion systems (magnetic Laval nozzle) and in fusion devices aiming to confine plasma and reach controlled thermonuclear fusion. We consider the linear stability of plasma flows under different boundary conditions. The linearized plasma equations are discretized and spectral stability problem is reduced to a polynomial eigenvalue problem. We found that the subsonic and supersonic flows are stable for Dirichlet boundary conditions. The subsonic flow is stable for the mixed (fixed-open) boundary conditions, but the supersonic flow is unstable. We show that different spectral methods, i.e. spectral collocation and spectral Galerkin methods, agree. Phenomena of spectral pollution resulting in spurious unstable modes is discussed. By studying the convergence of different modes, we successfully eliminated the spurious modes. The stability problem of the transonic velocity profile has an additional difficulty due to the singularity at the sonic point, i.e. at the point when the flow velocity is equal to the local sound velocity. At this point, the coefficient in front of the highest derivative of the differential eigenvalue equation becomes zero. In this case, the direct application of the spectral methods is problematic. To solve this problem, we solve the equation near the singularity by the Frobenius method and then use the regular solution with the shooting method to find the eigenvalues. We find that the transonic accelerating velocity profile is stable.

Chapter 1

Introduction

The title of this thesis involves several concepts, plasma, spectral instability, and magnetic nozzle. In the first chapter, we will introduce these concepts. Starting from the definition of plasma, then to the spectral instability and the general procedure of analyzing spectral instability. Following that, magnetic nozzle and magnetic mirror configuration will be introduced. After having these necessary knowledge, we are able to discuss the methods for analyzing the spectral instability of plasma flow in magnetic nozzle.

1.1 Plasma

Plasma is one of the fundamental states of matter, distinct from solid, liquid, and gas. In a plasma, the atoms or molecules have been stripped of electrons, resulting in a collection of charged particles, ions and electrons. In a vigorous sense, plasma is a fourth state of matter, though people often call it that way, because it does not involve phase transition. Plasma is the most common matter in the universe, it can be found in stars, including the sun, where nuclear fusion occurs at extremely high temperature. It also exists in solar wind, lightning and auroras. These natural plasmas can be seen in the sky because they are in plasma state, and plasma is capable of emitting light [9]. Plasma has various scientific and technology uses. The artificially generated plasma can be found in fluorescent lights, Neon signs, etc. It can also be found in plasma physics research, nuclear fusion experiments, plasma cutting and welding, plasma medicine for treating diseases, and even in spacecraft propulsion systems. Overall, plasma is an intriguing and versatile state of matter with significant implications in various fields of science, technology, and industry. Fig. 1.1 lists some commonly seen natural and artificial plasmas.
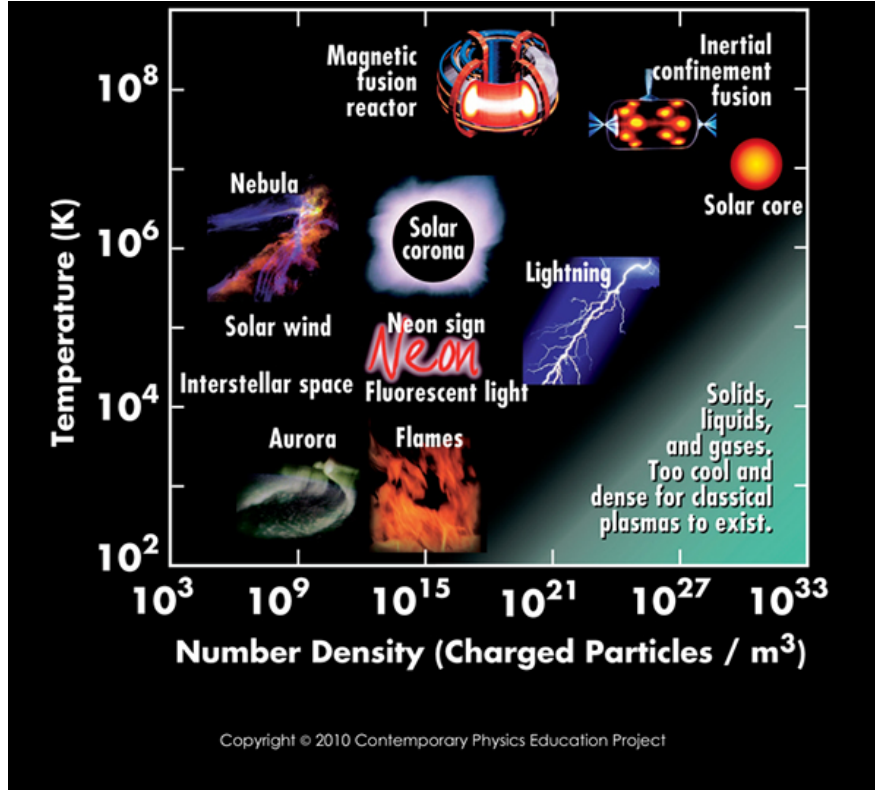
Figure 1.1: Typical plasmas. Adapted from [1].

1.1.1 Definition of Plasma

In simple terms, a plasma is an ionized gas which is quasineutral and exhibits collective behavior [9]. The following subsections will give precise definition of quasineutrality and collective behavior.

Debye Shielding and Quasineutrality

A key characteristic of plasma is its capability to shield external electric field. Imagine a positively charged ball is put into a plasma (Fig. 1.2, ions are neglected from the figure). Suppose there is sufficient amount of electrons in the plasma, and the plasma is cold, meaning that no thermal motions exist, the electric field generated by the ball will be shielded out by the surrounding electron cloud. If the plasma has finite temperature, then due to the thermal motions of electrons, the shielding will be incomplete and the edge of the electron cloud will be at the radius where potential energy is approximately equal to the thermal energy KT [9].

The Debye length is the thickness of the electron cloud. To find out Debye length, we need to compute the potential near the positively charged ball. Due to the symmetry of the

3
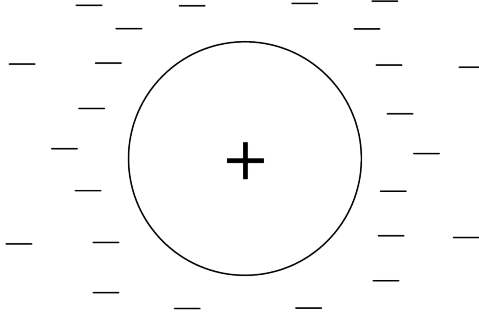
Figure 1.2: Debye shielding. Adapted from [9]. A positively charged ball is put into a plasma. Electrons will surround the ball. Ions are neglected from the picture since they are repelled away from the ball.

problem, we can reduce the it to 1D, along the radial direction. Suppose the coordinate's origin is at the ball's center and $\phi(0) = 0$. The potential can be solved from the following 1-dimensional Poisson's equation,

$$\epsilon_0 \frac{\mathrm{d}^2\phi}{\mathrm{d}x^2} = -e(n_i - n_e), \quad \phi(0) = \phi_0 \tag{1.1}$$

where n is the number density of the particles, and the subscripts i and e stand for ion and electron.

For simplicity, we assume massless electron, $m/M \to 0$. This means that the electrons move so fast that the ions can be treated as a static background. That is,

$$n_i = n_0 \tag{1.2}$$

where n_0 is a constant.

Meanwhile, it can be proven using Fluid description of plasma that the electron density follows the Boltzmann distribution,

$$n_e = n_0 \exp(e\phi/KT_e) \tag{1.3}$$

Taylor expand n_e in the region where $|e\phi/KT_e| \ll 1$ we have,

$$n_e = n_0 \left[1 + \frac{e\phi}{KT_e} + \frac{1}{2}\left(\frac{e\phi}{KT_e}\right)^2 + \cdots \right] \tag{1.4}$$

Substituting Eq. (1.2) and Eq. (1.4) for n_i and n_e in the 1D Poisson's equation, Eq. (1.1),

and only keep the linear terms in Eq. (1.4), we get

$$\epsilon_0 \frac{\mathrm{d}^2\phi}{\mathrm{d}x^2} = \frac{n_0 e^2}{KT_e}\phi \tag{1.5}$$

The solution to the Poisson's equation is therefore,

$$\phi = \phi_0 \exp(-|x|/\lambda_D) \tag{1.6}$$

where the quantity λ_D is called Debye length, and is defined as

$$\lambda_D \equiv \left(\frac{\epsilon_0 KT}{ne^2}\right)^{1/2} \tag{1.7}$$

where n stands for the number density far away from the charged ball. The potential is shown in Fig. 1.3. The Debye length characterizes the thickness the of the cloud.
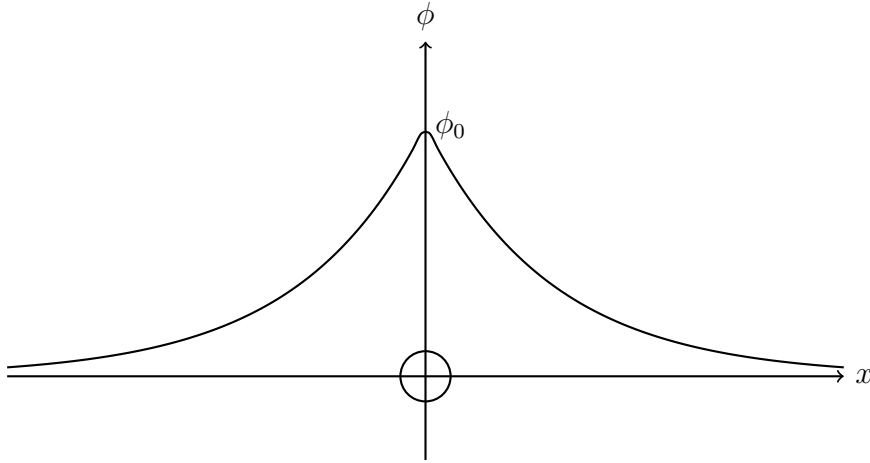
Figure 1.3: Potential distribution near a positively charged ball in a plasma. Adapted from [9]. The charged ball is centered at the origin, the potential generated by this ball decreases exponentially.

The above discussion indicates that any external electric field present in a plasma will be shielded out within a distance λ_D (assuming the system size L is much larger than λ_D). Therefore, the plasma stays neutral if it is initially electrically neutral.

A plasma is said to be quasineutral, if a plasma is neutral enough so that we can take $n_i \simeq n_e$ but a small charge imbalance can give rise to potentials of the order of KT/e. In this case, we can the symbol n to denote the common density and call it the plasma density [9].

Plasma Oscillation

Simply speak, the collective behavior of a plasma is mostly governed by the electromagnetic forces rather than the gas dynamics. To quantify this statement, we introduce the concept of plasma oscillation.

There are many kinds of oscillations in plasma, one of the most fundamental oscillations is the electron plasma oscillation. Imagine the ions are too heavy to move, and they form a uniform background. The electrons are then released from a distance away from the ions (Fig. 1.4). The electric field will pull the electrons toward the ions, after the electrons pass the ions, the electric field will decelerate them and started to pull them on the other side. The frequency of this oscillation is called plasma frequency,

$$\omega_p = \left(\frac{n_0 e^2}{\epsilon_0 m}\right)^{1/2} \tag{1.8}$$
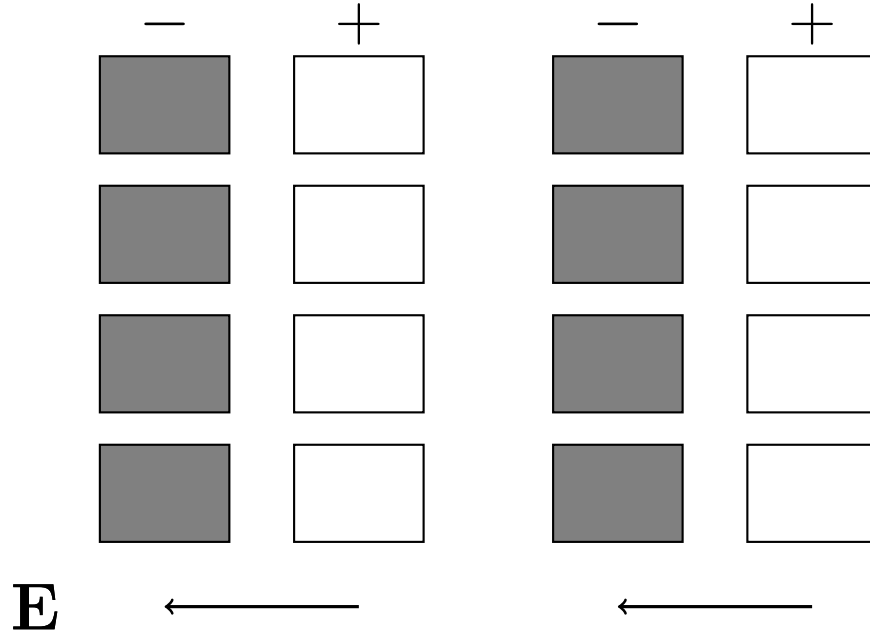
Figure 1.4: Mechanism of plasma oscillations. Adapted from [9]. As the electrons are pulled away from the ions, electric field forms and will pull the electrons back to the equilibrium position. Hence oscillation happens.

Criteria of Plasma

We are now able to give more detail definition for plasma. According to [9], not all ionized gas can be called plasma, there are three conditions a plasma must satisfy:

1. Debye length is much smaller than the system size, $\lambda_D \ll L$.

2. Collective behavior requires lots of particles in a Debye sphere, $N_D = n\frac{4\pi}{3}\lambda_D^3 \ggg 1$.

3. The ionized gas behaves like plasma rather than a neutral gas, $\omega_p\tau > 1$ where ω_p typical plasma oscillation frequency and τ is the mean free time of collisions between neutral atoms.

1.2 Instability of Plasma

The instability of plasma refers to the tendency of a plasma system to deviate from a stable, equilibrium state and exhibit perturbations or fluctuations in its behavior. It can be understood as the simple mechanical analogy with a ball on crest / in valley. On the left of Fig. 1.5 shows us a stable equilibrium, small perturbations given to the system will not push the ball far away from the equilibrium position, the valley. Hence, the equilibrium is stable. On the right, any small perturbations will cause the ball to fall downhill, hence the equilibrium is unstable. The instabilities in plasma can arise from various factors, such as the interaction of particles with electromagnetic fields, collective effects, or the presence of gradients in plasma parameters. A famous example of instability is the two stream instability. The configuration starts with two oppositely traveling beams of ions and electrons. As time evolves, chaotic behavior develops as shown in Fig. 1.6.

(a) Stable equilibrium.   **(b)** Unstable equilibrium.
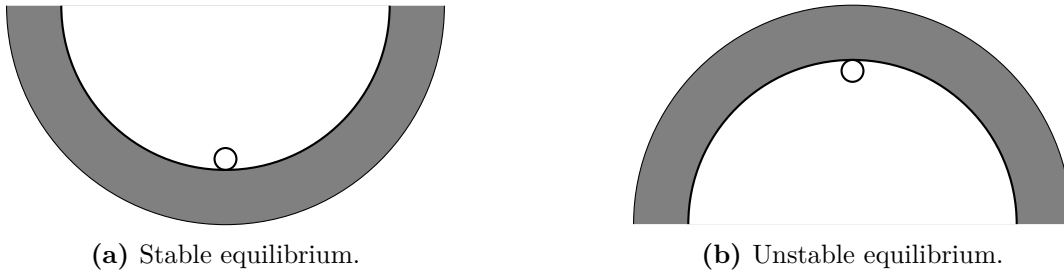
Figure 1.5: Mechanical analogy of various types of equilibrium. Adapted from [9].

Magnetic nozzle is one of the most actively researched configurations in plasma propulsion systems, which is being developed for space missions due to their potential for high efficiency and thrust. Understanding and controlling instabilities in the plasma flow within these nozzles is essential for optimizing their performance and achieving efficient propulsion. Investigating instabilities in plasma flow within magnetic nozzles also contributes to our broader understanding of fundamental plasma physics phenomena.
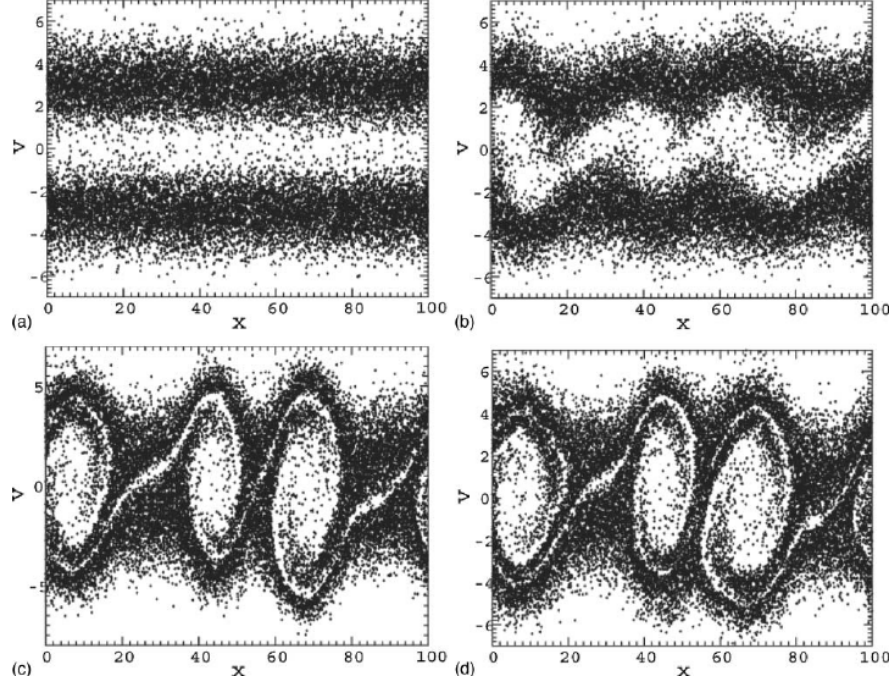
Figure 1.6: Visualization of two-stream instability in the phase space. (a) Initially the ion and electron flow are in opposite direction. (b) The velocity of both flows start to oscillate. (c) Chaotic behavior occurs. (d) The chaotic behavior continues. Adapted from [16].

1.2.1 Analysis of Spectral Instability

In this thesis, we will focus on the so-called linear instability. Meaning that the perturbation grows / decays only in exponential form. The following is a brief description of the process for analyzing linear instability. The detail treatment will be given in Chap. 2.

1. State equations of motion: The linear instability analysis starts from the equations of motion which describes the plasma system. In this thesis, the equations of motion are time-dependent fluid equations involving the number density n and velocity v of the plasma flow along the central axis of the nozzle.

2. Give perturbations to the system: Suppose the system has an equilibrium state n_0 and v_0. The system will be given small perturbations, they serve as small deviations on number density and velocity, $\tilde{n}$ and $\tilde{v}$. All variables n and v in the equations of motion will be substituted by perturbed quantities, $n_0 + \tilde{n}$ and $v_0 + \tilde{v}$.

3. Linearize equations of motion: Expand the equations of motion, and discard the second and higher order terms, often called nonlinear terms, such as $\tilde{n}\tilde{v}$, $\tilde{n}\partial_z\tilde{v}$, $\tilde{v}\partial_z\tilde{n}$ etc. We obtain the so-called linearized equations of motion. These equations contain only the linear terms.

8

4. Assume perturbation takes exponential form: Let perturbations take the form $\exp(-i\omega t)$. This indicates that the perturbations are oscillating with frequency ω in time. Any time derivative in the linearized equations of motion simply becomes $\partial_t = -i\omega$. Now we obtain equations involving perturbations, $\tilde{n}$ and $\tilde{v}$, and their spatial derivatives, and ω.

5. Analyze the possible values of ω: The oscillation frequency ω could be a complex number. If the imaginary part of the temporal frequency is greater than zero, i.e. $\text{Im}(\omega) > 0$, then the system is unstable. This is because the perturbation grows exponentially $\exp(\text{Im}(\omega)t)$ in time. On the other hand, if the imaginary part of the temporal frequency is less than or equal to zero, $\text{Im}(\omega) \leq 0$, then the system is said to be stable. Since the perturbations will not be growing, $\text{Im}(\omega) = 0$, or even damped, $\text{Im}(\omega) < 0$.

In the later chapters, we devoted much effort to analyze the temporal frequency ω. We will employ spectral method to analyze the temporal frequency for subsonic and supersonic velocity profiles, and shooting method will be employed to obtain temporal frequency.

1.3 Magnetic Nozzle

In this thesis, we are going to deal with plasma flow in magnetic nozzle. A magnetic nozzle is a device that uses a magnetic field to shape and control the flow of charged particles in a plasma propulsion system, see Fig. 1.7. By employing magnetic mirrors, the magnetic nozzle can efficiently direct and accelerate the plasma particles, generating thrust for propulsion. The magnetic field in the nozzle helps collimate and focus the plasma exhaust, increasing its velocity and enhancing the performance of the propulsion system.

1.3.1 Magnetic Field in Magnetic Nozzle

The magnetic nozzle by its nature is 3-dimensional. We assume the magnetic field is axis-symmetric, then the radial magnetic field and axial magnetic field are constraint by divergence-free condition,

$$\boldsymbol{\nabla} \cdot \mathbf{B} = \frac{1}{r}\frac{\partial(rB_r)}{\partial r} + \frac{\partial B_z}{\partial z} = 0 \tag{1.9}$$

Since we are interested in the plasma flow near the central axis of the nozzle, with paraxial approximation taken, the derivative along the magnetic field line $\nabla_\parallel = \partial/\partial z$ when near the central axis [31]. Hence, in this thesis we will treat the flow in magnetic nozzle as a
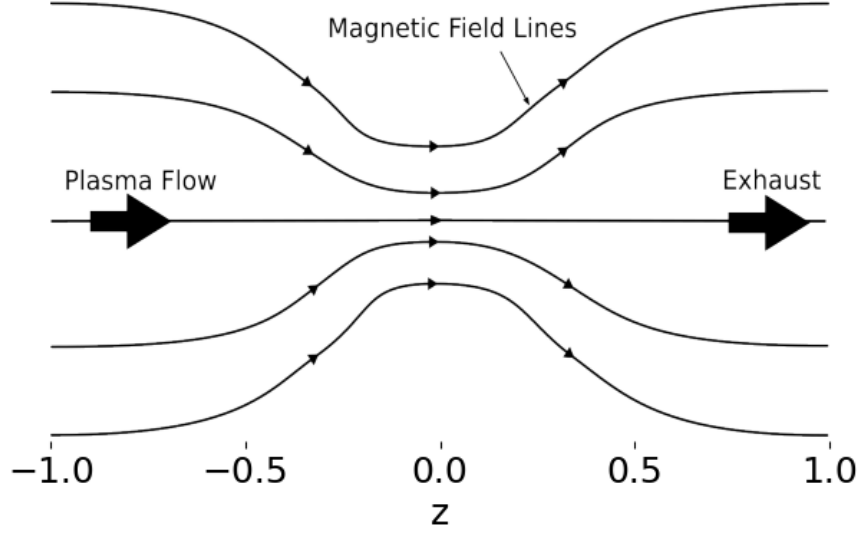
Figure 1.7: A simplified example of a magnetic nozzle configuration. On the left ($z = -1$) is the entrance of the nozzle. The plasma flows into the nozzle from the left and will be accelerated and finally exhaust through the exit on the right ($z = 1$). The magnetic field lines are shaped in such a way that it forms a magnetic mirror configuration. Plasma flow with specific subsonic speed at the entrance will be accelerated to supersonic speed.

1-dimensional problem. The axial magnetic field along the central axis is modeled as

$$B_z(z) = B_0 \left[1 + R \exp\left(-\left(\frac{z}{\delta}\right)^2 \right) \right], \quad -1 \leq z \leq 1 \tag{1.10}$$

where $1 + R$ is the magnetic mirror ratio, it is the ratio of the magnitude of magnetic field at the center of the nozzle to that at the end of the nozzle, $1 + R = B(0)/B(1)$. The mirror ratio R controls the spread of the plasma flow at the exit. On the other hand, δ determines the spread of the magnetic field. Larger the δ, flatter the magnetic field. An example of magnetic field is shown in Fig. (1.8).

The radial profile of magnetic field, B_r, is given by the divergence-free condition, Eq. (1.9). In this thesis will focus on the axial magnetic field only.

1.3.2 Velocity Profiles of Plasma Flow in Magnetic Nozzle

The analytical solution gives 4 different kinds of velocity profiles,

- Subsonic profile: Plasma flow enters and exits the nozzle with subsonic speed. Every point on this profile is subsonic.

- Supersonic profile: Plasma flow enters and exits the nozzle with supersonic speed. Every point on this profile is supersonic.
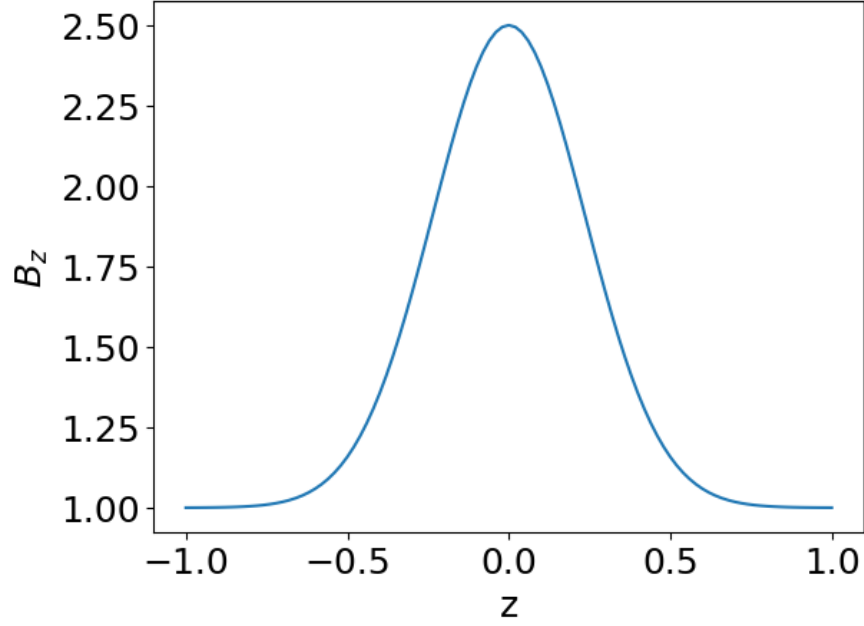
Figure 1.8: This is the magnetic field in nozzle with mirror ratio $1 + R = B_{max}/B_{min} = 2.5$, and the spread of magnetic field, $\delta = 0.1/0.3 = 0.\bar{3}$.

- Accelerating profile: Plasma flow enters the nozzle with subsonic speed and exits the nozzle with supersonic speed. Points before the nozzle throat are subsonic, and the flow reaches ion sound speed at the nozzle throat, then the flow is supersonic after the nozzle throat.

- Decelerating profile: Plasma flow enters the nozzle with supersonic speed and exits the nozzle with subsonic speed. Similar to the accelerating profile, but the velocity is decreasing.

See Fig. 2.4 for these profiles.

The velocity of plasma flow in the magnetic nozzle is given by the Lambert W function, Eq. (2.32). The Lambert W function has 2 different branches. The $k = 0$ branch corresponds to the subsonic parts in the velocity profile, and the $k = -1$ branch gives the supersonic parts. The expression of velocity profile will be derived in Chap. 2 and more details will be discussed.

1.4 Flow in Similar Configuration: Bondi-Parker Flow

Consider a massive celestial object in the space. This celestial object will attract matter in the space because it is massive. Hence, creating an accretion flow. If the celestial object is a star, it can also eject matter into space. Solar wind is an example to this since it is a stream

of charged particles, primarily electrons and protons, flowing outward from the Sun. Bondi derived a steady-state solution for accretion flow which is governed by Bernoulli's equation in spherical symmetry around a point mass in 1952. Hence, the inward accretion flow is also called Bondi flow. Then Parker solved a similar problem but with outward wind in 1958. Then the outward wind is given the name, Parker flow [3, 5, 19]. The Bondi and Parker flow (also called Bondi-Parker flow) is similar to that in magnetic nozzle. It is interesting to compare the two configurations.

If we compare the velocity profiles for Bondi-Parker flow and the flow in magnetic nozzle. We found they are similar. The Bondi-Parker flow can also be grouped into the following types: subsonic, supersonic, and transonic (accelerating and decelerating). See Fig. 1.9. For subsonic profiles, every point on the curve is slower than sound speed. While every point on the supersonic velocity profile is faster than sound speed. Lastly, there are two different transonic profiles: accelerating profile and decelerating profile. The accelerating profile describes the accelerating plasma flow which is at subsonic speed at the mass point, e.g. a star, and is accelerated to supersonic speed far away. The decelerating profile shows that a plasma flow ejected supersonically from a mass point and then decelerated to subsonic speed far away.

The velocity profiles of one-dimensional, spherically symmetric, stationary isothermal Parker flow neglecting self-gravity can be expressed using Lambert W function,

$$v(r) = \sqrt{-\frac{KT}{m}W_k\left[-\left(\frac{r}{r_c}\right)^2 \exp\left[4\left(1 - \frac{r_c}{r}\right) - 1\right]\right]}, \quad k = 0, -1 \qquad (1.11)$$

where r stands for the distance measured from the center of the mass point, e.g. star. The position $r_c = GMm/2KT$ is the critical position and the velocity at this point is exactly the sonic speed $v(r_c) = \sqrt{KT/m}$, where M is the mass of the mass point, m is the mass of a single particle in the flow, and T is the temperature of the flow. The Bondi flow is simply $-v(r)$ since it is accretion flow, the particles are flowing inwardly towards the mass point.

As we can see the expression of velocity profile for Bondi-Parker flow is similar to that of the magnetic nozzle, Eq. (2.32). The expression is governed by the Lambert W function. Similarly, the $k = 0$ branch corresponds to the subsonic part in the velocity profile, and the $k = -1$ branch corresponds to the supersonic part of the profile.

The instabilities of the Bondi-Parker flow has been extensively studied [5, 37, 38, 12, 19]. Hopefully these studies can provide insights into our problem.
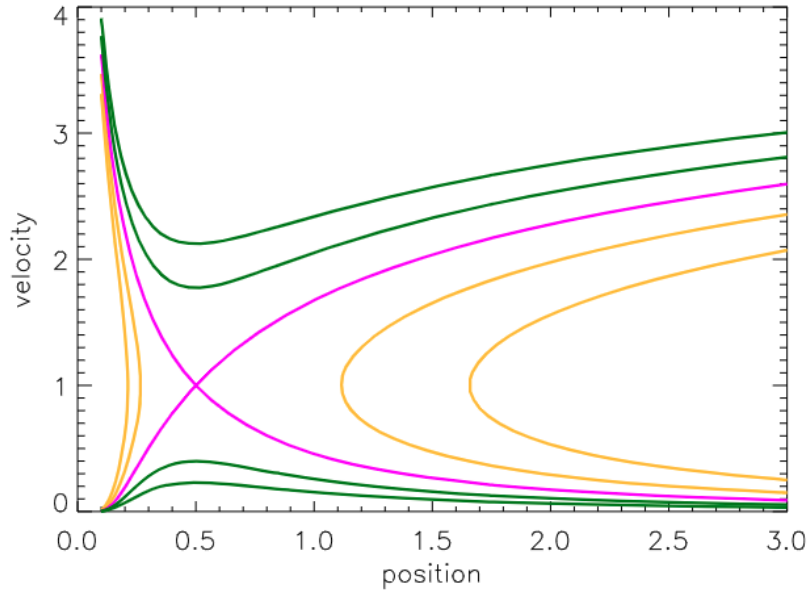
Figure 1.9: Representative trajectories of the steady-state BP flow in non-dimensional units. The velocities are shown in absolute values. Adapted from [19]. The upward pink line represents an accelerating flow, it accelerates from subsonic to supersonic. The downward pink line represents a decelerating flow. The green lines below the pink lines represent subsonic flows, and the green lines above represent supersonic flows. Orange lines are physically impossible scenarios. If the sign of the velocity is positive, then it is an outward (Parker) flow, otherwise it is an inward (Bondi) flow.

1.5 Goals of this Thesis

Fusion is considered the next-generation source of a clean, safe and abundant energy providing an opportunity to address climate change problems. A new high-tech industry has appeared in the last decade fueled by over $4 billion of private investments, with the second world largest and several other smaller companies founded in Canada. To achieve controlled fusion, one of the key science problems is to understand and learn to predict the non-linear behavior of plasma due to waves and instabilities. The general objective of my research is to understand the behavior and learn to control the turbulent flows of plasmas in magnetically controlled fusion system, in particular, open magnetic mirrors. I study the instabilities of the flow in a magnetic mirror configuration under different boundary conditions which is an open question and is under debate in application to fusion systems and also related to the solar wind flows.

The general objective of this research is to understand the stability of the flow in a magnetic nozzle. Plasma confined by the magnetic field is typically far from the state of the thermodynamic equilibrium which makes it unstable. In this project, we would like to investigate the stability of plasma flow in a magnetic nozzle under different boundary conditions. Understanding the instabilities of plasma flow in a magnetic mirror configuration is important in applications such as the expanding magnetic divertors in controlled fusion and electric propulsion [29, 18].

In the following thesis, fluid model of plasma will be reviewed and linearized governing equations will be derived in chapter 2. The problem will be then formulated as an eigenvalue problem. In chapter 3, spectral method for solving eigenvalue problem will be introduced. Spectral-collocation and spectral-Galerkin methods will be discussed. Moreover, spectral pollution and the filtering techniques will as also be investigated. If the velocity profile is transonic, the existence of singularity at the nozzle throat prevents the use the spectral methods, therefore we will formulate the problem to the form suitable for applying shooting method. In chapter 4 we will discuss the existence of the singularity and then extract the regular solutions using Frobenius method. After this, we will apply shooting method to the problem and investigate the instabilities. Conclusion will in chapter 5.

Chapter 2

Polynomial Eigenvalue Problem

Magnetic field lines guide the motion of charged particles in plasma. In this chapter, we first examine the single particle motion along the magnetic field, subsequently to a kinetic description of plasma. Following this, we derive the fluid description of plasma using the fact that fluid velocity follows the magnetic field line $\mathbf{v} = v\mathbf{B}/B$. After this, we establish the governing equations for flow in the magnetic nozzle. Following their derivation, we proceed to linearize these governing equations and reframe the problem as a polynomial eigenvalue problem. Finally, we analytically explore a special case.

2.1 Kinetic Theory

2.1.1 Single Particle Motion in Uniform Magnetic and Electric Fields

Plasma consists of charged particles, and is governed by electromagnetic force. This subsection gives a description of single particle motion with the presence of uniform magnetic and electric fields. This gives us intuition of how the particles move in a magnetic nozzle. Since the particle motion is governed by Lorentz force, the equation of motion of a charged particle is given by

$$m\frac{\mathrm{d}\mathbf{v}_p}{\mathrm{d}t} = q(\mathbf{E} + \mathbf{v}_p \times \mathbf{B}) \tag{2.1}$$

where m is the mass of charged particle, q is its electric charge, and $\mathbf{v}_p$ is the particle's velocity.

No Electric Field

Consider a uniform magnetic field pointing in z-direction, $\mathbf{B} = B\hat{\mathbf{z}}$, and no electric field for now. Since the magnetic force is perpendicular to both $\mathbf{v}_p$ and $\mathbf{B}$, we can separate the equation of motion into two directions,

$$m\frac{d\mathbf{v}_\parallel}{dt} = \mathbf{0}$$
$$m\frac{d\mathbf{v}_\perp}{dt} = q\mathbf{v}_\perp \times \mathbf{B} \tag{2.2}$$

where $\mathbf{v}_\parallel$ denotes the velocity along the magnetic field line, in this case $v_\parallel = v_z$, and $\mathbf{v}_\perp$ is the velocity perpendicular to the magnetic field, in this case $\mathbf{v}_\perp = v_x\hat{x} + v_y\hat{y}$. Solving these equations with initial condition $\mathbf{v_p}|_{t=0} = v_{0x}\hat{x} + v_{0y}\hat{y} + v_{0z}\hat{z}$ we get

$$v_x = v_{0\perp}e^{i\omega_c t}$$
$$v_y = \pm i v_{0\perp}e^{i\omega_c t} \tag{2.3}$$
$$v_z = v_{0z}$$

where $v_{0\perp} = \sqrt{v_{0x}^2 + v_{0y}^2}$ is the initial speed in the plane perpendicular to the magnetic field, and $\omega_c \equiv |q|B/m$ is called the Larmor frequency. In this way, we see that the charged particle is doing circular motion in the $x-y$ plane with Larmor frequency ω_c. On the other hand, the particle is flowing freely in $\hat{z}$ direction since there is no force acting on the charged particle along the magnetic field line. The charged particle is doing helical motion along the magnetic field line. See Fig. 2.2. If we integrate the velocities with respect to time we will see the radius of the gyration is a constant, $r_L \equiv m_v \perp /|q|B$, it is called Larmor radius.

Finite Electric Field

With the presence of uniform electric field $\mathbf{E} = E_x\hat{x} + E_y\hat{y} + E_z\hat{z}$, the solution to Eq. (2.1) becomes

$$v_x = v_{0\perp}e^{i\omega_c t} + \frac{E_y}{B}$$
$$v_y = \pm i v_{0\perp}e^{i\omega_c t} - \frac{E_x}{B} \tag{2.4}$$
$$v_z = v_{0z} + \frac{qE_z}{m}t$$

In the direction along the magnetic field, electrostatic force is acting on the particle causing it to accelerate / decelerate with constant acceleration qE_z/m. In the direction perpendicular

16

to magnetic field, the Larmor radius is still $r_L = m_{v \perp}/|q|B$ but the particle's guiding center drifts with velocity

$$\mathbf{v_{E \times B}} = \frac{\mathbf{E} \times \mathbf{B}}{B^2} = \frac{E_y}{B}\hat{x} - \frac{E_x}{B}\hat{y} \tag{2.5}$$

This is so-called the $\mathbf{E} \times \mathbf{B}$ drift.

Imagine a cylinder shape magnetic nozzle with externally applied magnetic field, the magnetic field is as described in Sec. 1.3.1. The particles will move along the magnetic field lines. Due to high mobility of electrons, they move faster than ions, this creates electric field and will accelerate ions in the nozzle (more details will be discussed in Sec. 2.2). By symmetry, if there is electric field in the plane perpendicular to $\mathbf{B}$ field, it will be pointing radially, $\mathbf{E}_\perp = E_\perp \cos\theta\hat{x} + E_\perp \sin\theta\hat{y}$. According to the above discussion, the $\mathbf{E} \times \mathbf{B}$ drift, $\mathbf{v_{E \times B}} = E_\perp/B(\sin\theta\hat{x} - \cos\theta\hat{y})$, will be in $\hat{\theta}$ direction. Meaning that in magnetic nozzle, the particles have two gyrating motions: one is the small scale Larmor gyration, and the other one is the larger scale $\mathbf{E} \times \mathbf{B}$ drift in $\hat{\theta}$ direction. In this thesis, we are interested in the flow near the central axis, therefore the larger scale drift will be ignored.

2.1.2 Adiabatic Invariants

The charged particles always travel on the same magnetic field line in the magnetic nozzle. To show this we will introduce two adiabatic invariants.

Magnetic Moment

In classical mechanics, the action integral $\oint p\,dq$ taken over a period of a periodic motion is a constant. Here p and q are generalized momentum and coordinate. In single particle motion along magnetic field line, one obvious periodic motion is the Larmor gyration. Take p to be the angular momentum $mv_\perp r$ and q to be the angular coordinate θ, the action integral becomes

$$\oint p\,dq = \oint mv_\perp r_L d\theta = 2\pi r_L mv_\perp = 2\pi\frac{mv_\perp^2}{\omega_c} = 4\pi\frac{m}{|q|}\left(\frac{mv_\perp^2}{2B}\right) \tag{2.6}$$

Define the quantity magnetic moment as

$$\mu = \frac{mv_\perp^2}{2B} \tag{2.7}$$

We see that the magnetic moment μ is constant as long as q/m is constant.

17

Longitudinal Invariant

The next adiabatic invariant is the quantity defined as [9]

$$J = \int_a^b v_\parallel ds \tag{2.8}$$

where a and b are the two turning points in magnetic mirror, see Fig. 2.1.
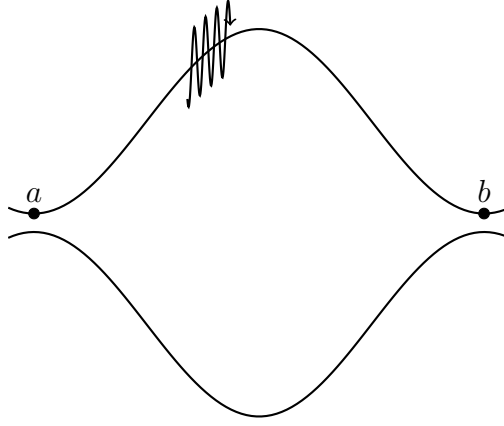
Figure 2.1: A particle bouncing between turning points a and b in a magnetic field. Adapted from [9].

Since the particle's energy is conserved and is equal to $mv_\perp^2/2$ at the turning point, the invariance of μ indicates that $|B|$ remains the same at the turning point. However, upon drifting back to the same longitude, a particle may find itself on another line of force at a different altitude. This cannot happen if J is conserved. J determines the length of the line of force between turning points, and no two lines have the same length between points with the same $|B|$. Consequently, the particle returns to the same line of force even in a slightly asymmetric field.

2.1.3 From Kinetic Theory to Fluid Description

Although the previous treatment is useful for single particle, to describe the collective behavior of a large amount of particles, we need to do that in the framework of kinetic theory. In kinetic theory, the charged particles in plasma obey a certain velocity distribution function,

$$f(\mathbf{x}, \mathbf{v}_p, t) \tag{2.9}$$

18
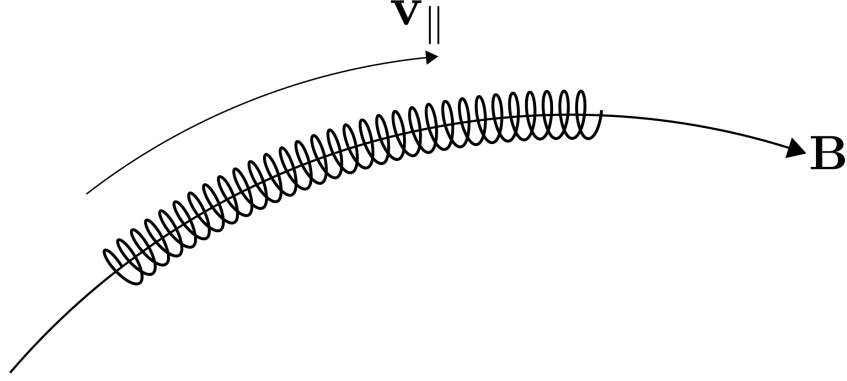
Figure 2.2: A charged particle gyrates about the magnetic field line. The velocity along the field line is $\mathbf{v}_\parallel$ and the gyrate frequency, radius is given by the radial equation, $q\mathbf{v}_\perp \times \mathbf{B} = \hat{\mathbf{r}}mv_\perp^2/r$. Moreover, for static, nonuniform magnetic field, the charged particle will stay on the same of magnetic field line as it gyrates.

The number of particles per m^3 at position $\mathbf{x}$ and time t with velocity components in the cell bounded by $\mathbf{v}$ and $\mathbf{v} + d\mathbf{v}$ is

$$f(\mathbf{x}, \mathbf{v}_p, t)d^3\mathbf{v}_p \tag{2.10}$$

Suppose a collisionless plasma in 3-dimensional space is at thermal equilibrium, then the particles can be characterized by Maxwell-Boltzmann distribution

$$f_M(\mathbf{x}, \mathbf{v}_p, t) = \frac{n(\mathbf{x}, t)}{(\pi v_{th}^2)^{3/2}} \exp\left(-\left(\frac{v}{v_{th}}\right)^2\right)$$

where $n(\mathbf{x}, t)$ is number density of the particles, $v_{th} = \sqrt{2k_BT/m}$ is the thermal velocity, and $v = \sqrt{v_x^2 + v_y^2 + v_z^2}$.

The moments of the distribution function are suitable macroscopic properties of the plasma. For example, the plasma number density and momentum can be viewed as

$$\begin{aligned} n(\mathbf{x}, t) &= \int_{\mathbb{R}^3} f(\mathbf{x}, \mathbf{v}_p, t)d^3\mathbf{v}_p \\ n\mathbf{v}(\mathbf{x}, t) &= \int_{\mathbb{R}^3} \mathbf{v}_p f(\mathbf{x}, \mathbf{v}_p, t)d^3\mathbf{v}_p \end{aligned} \tag{2.11}$$

where $\mathbf{v}$ without the subscript p is the fluid velocity of the plasma flow. It is the bulk velocity of the plasma. The charged particles flow along the magnetic field line, it is intuitive to think of $\mathbf{v}$ as the plasma flow velocity along the magnetic field line.

In this thesis we assume collisionless plasma. The distribution function f in a collisionless

plasma satisfies the so-called collisionless Vlasov equation, $\mathrm{d}/\mathrm{d}t\, f(\mathbf{x}, \mathbf{v}, t) = 0$. Expand it explicitly, it is

$$\frac{\partial f}{\partial t} + \mathbf{v}\frac{\partial f}{\partial \mathbf{x}} + \frac{q}{m}(\mathbf{E} + \mathbf{v} \times \mathbf{B})\frac{\partial f}{\partial \mathbf{v}} = 0 \tag{2.12}$$

where $q(\mathbf{E} + \mathbf{v} \times \mathbf{B})$ is the Lorentz force experience by the species, the collision term $C(f)$ is dropped.

Integrate both sides with respect to volume element in velocity space, $d^3\mathbf{v}$, we get the conservation of density.

$$\frac{\partial n}{\partial t} + \boldsymbol{\nabla} \cdot (n\mathbf{v}) = 0 \tag{2.13}$$

If we multiply $\mathbf{v}$ on both sides and integrate with respect to $d^3\mathbf{v}$, we get the conservation of momentum.

$$mn\left[\frac{\partial \mathbf{v}}{\partial t} + (\mathbf{v} \cdot \boldsymbol{\nabla})\mathbf{v}\right] = qn(\mathbf{E} + \mathbf{v} \times \mathbf{B}) - \boldsymbol{\nabla} \cdot \mathbf{P} + \mathbf{P}_{ij} \tag{2.14}$$

where $\mathbf{P} \equiv mn\overline{\mathbf{v}}_{thermal}\overline{\mathbf{v}}_{thermal}$, the bar represents average over velocity space with distribution function $f(\mathbf{x}, \mathbf{v}_p, t)$, is the stress tensor. If we assume isothermal plasma with isotropic pressure, $p = nKT$ where T is constant, then the last two terms can be simplified to $\boldsymbol{\nabla}p = KT\boldsymbol{\nabla}n$.

As we can see the fluid description only depends on the macroscopic properties of plasma, such as the fluid velocity along the magnetic field line $\mathbf{v}$, number density n, and pressure p of the plasma. This simplifies the problem.

2.2   Equation of Motion of the Plasma Flow in Nozzle

In this section, we will derive the governing equations of the quasineutral plasma flow with cold magnetic ions in magnetic nozzle under paraxial approximation.

Starting from the conservation of number density,

$$\frac{\partial n}{\partial t} + \boldsymbol{\nabla} \cdot (n\mathbf{v}) = 0 \tag{2.15}$$

Since ions carry most of the mass and momentum in the plasma, their velocity is more representative of the bulk flow of the plasma. Electrons, on the other hand, have much smaller mass and are highly mobile due to their low inertia, but they contribute less to the overall momentum of the flow. As we discussed in the Sec. 2.1.1, the charged particles are doing helical motions along the magnetic field lines. Hence, we take the fluid velocity as the ion velocity along the magnetic field lines

$$\mathbf{v} = v\mathbf{B}/B \tag{2.16}$$

By expanding the divergence term $\boldsymbol{\nabla}\cdot(n\mathbf{v})$, and using the divergence free condition $\boldsymbol{\nabla}\cdot B = 0$, we have

$$\frac{\partial n}{\partial t} + \mathbf{B} \cdot \boldsymbol{\nabla}\left(\frac{nv}{B}\right) = 0 \tag{2.17}$$

Using the paraxial approximation, $\boldsymbol{\nabla}_{\parallel} = \partial_z \hat{z}$. We obtain the conservation of density for the magnetic nozzle,

$$\frac{\partial n}{\partial t} + B\frac{\partial}{\partial z}\left(\frac{nv}{B}\right) = 0 \tag{2.18}$$

The conservation of momentum for ions and electrons are

$$m_i n \left[\frac{\partial \mathbf{v}}{\partial t} + (\mathbf{v} \cdot \boldsymbol{\nabla})\mathbf{v}\right] = en(\mathbf{E} + \mathbf{v} \times \mathbf{B}) \tag{2.19}$$

$$m_e n \left[\frac{\partial \mathbf{v}}{\partial t} + (\mathbf{v} \cdot \boldsymbol{\nabla})\mathbf{v}\right] = -en(\mathbf{E} + \mathbf{v} \times \mathbf{B}) - \boldsymbol{\nabla}p_e \tag{2.20}$$

where p_e is the electron pressure. There are some simplifications, first is that the term $\mathbf{v} \times \mathbf{B} = 0$ due to the fact that fluid velocity is along $\mathbf{B}$. Secondly, $m_e n \frac{d\mathbf{v}}{dt} \simeq 0$ due to small electron mass. Hence, the above two equations becomes,

$$m_i n \left[\frac{\partial v}{\partial t} + v\frac{\partial v}{\partial z}\right] = enE_{\parallel} \tag{2.21}$$

$$0 = -enE_{\parallel} - \frac{\partial p_e}{\partial z} \tag{2.22}$$

Adding these two equations we obtain

$$\frac{\partial v}{\partial t} + v\frac{\partial v}{\partial z} = -\frac{1}{m_i n}\frac{\partial p_e}{\partial z} \tag{2.23}$$

Assume isothermal, then the electron pressure, also called the equation of state, is

$$p_e = nKT_e \tag{2.24}$$

We can make this assumption due to the fact the electrons are so mobile that their heat conductivity is almost infinite. [9]

Therefore, we have

$$\frac{\partial v}{\partial t} + v\frac{\partial v}{\partial z} = -c_s^2\frac{1}{n}\frac{\partial n}{\partial z} \tag{2.25}$$

where $c_s^2 = KT_e/m_i$ is the square of ion sound speed.

Therefore, the dynamics of the plasma flow in magnetic nozzle can be characterized by

the conservation of density and momentum,

$$\frac{\partial n}{\partial t} + B\frac{\partial}{\partial z}\left(\frac{nv}{B}\right) = 0$$

$$\frac{\partial v}{\partial t} + v\frac{\partial v}{\partial z} = -c_s^2\frac{1}{n}\frac{\partial n}{\partial z}$$

The magnetic field profile was discussed in Sec.1.3.1.

From the above derivation, it is clear that due to finite temperature and high mobility of the electrons, they establish the electric field to accelerate the cold magnetized ions in the nozzle. The thermal energy of the electrons are converted to kinetic energy of ions in this setup.

For convenience, we nondimensionalize the governing equations by normalizing the velocity to c_s, $v \mapsto v/c_s$, z to system length L, $z \mapsto z/L$ and time $t \mapsto c_s t/L$. The governing equations become

$$\frac{\partial n}{\partial t} + n\frac{\partial v}{\partial z} + v\frac{\partial n}{\partial z} - nv\frac{\partial_z B}{B} = 0 \tag{2.26}$$

$$n\frac{\partial v}{\partial t} + nv\frac{\partial v}{\partial z} = -\frac{\partial n}{\partial z} \tag{2.27}$$

In the later thesis, we will refer the governing equations to Eq. (2.26), (2.27) without mentioning the nondimensionalization.

2.3 Velocity Profiles at Equilibrium

2.3.1 Lambert W Function

Lambert W function is necessary for the following discussion.

Definition 1. The Lambert W function is a function, $y(x)$, such that $ye^y = x$ holds, where $x, y \in \mathbb{R}$.

It is denoted as $W_k(x)$, where $k = 0, -1$ are its two branches. See Fig. 2.3.

2.3.2 Velocity Profiles

In this research, we are interested in the stability of such plasma flow in the nozzle at equilibrium. Let's denote n_0 and v_0 as equilibrium density and equilibrium velocity, respectively. Since they are stationary (time independent) solutions to the governing equations Eq. (2.26),
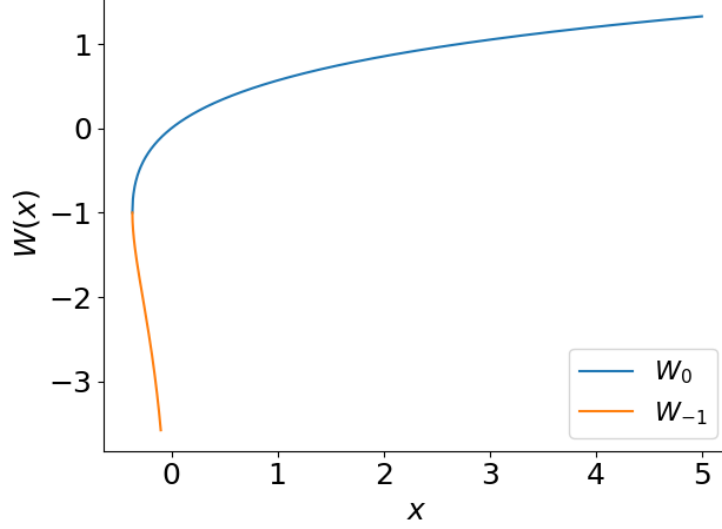
Figure 2.3: The graph of $y = W(x)$ for real $x < 5$ and $y > -4$. The upper branch (blue) with $y \geq -1$ is the graph of the function $W_0(x)$ (principal branch), the lower branch (orange) with $y \leq -1$ is the graph of the function $W_{-1}(x)$. The left most point of the curve is at $(-1/e, -1)$.

(2.27), they satisfy the so-called equilibrium condition (nondimensionalized),

$$\frac{\partial}{\partial z}\left(\frac{n_0 v_0}{B}\right) = 0 \tag{2.28}$$

$$v_0 \frac{\partial v_0}{\partial z} = -\frac{1}{n_0}\frac{\partial n_0}{\partial z} \tag{2.29}$$

In this section we will solve the equilibrium velocity profile, v_0, from the nondimension-alized equilibrium condition, Eq. (2.28) and Eq. (2.29). We start by substituting $\frac{1}{n_0}\,\partial n_0/\partial z$ into Eq. (2.28), then it becomes

$$(v_0^2 - 1)\frac{\partial v_0}{\partial z} = -\frac{v_0}{B}\frac{\partial B}{\partial z} \tag{2.30}$$

Notice that there is a singularity at $v_0 = 1$, the sonic speed. Later we will devote an entire Chap. 4 to discuss the treatment for solving eigenvalues involving this singularity.

We can solve the equation by separating the variables, i.e. v_0 on one side and B on the other side of the equal sign. Then integrate equation with respect to z and use the conditions at midpoint $B(0) = B_m, v_0(0) = v_m$ we get

$$v_0^2 e^{-v_0^2} = \frac{B^2}{B_m^2}v_m^2 e^{-v_m^2} \tag{2.31}$$

We can now express v_0 using the Lambert W function,

$$v_0(z) = \left[-W_k \left(-\frac{B(z)^2}{B_m^2} v_m^2 e^{-v_m^2} \right) \right]^{1/2} \tag{2.32}$$

where the subscript k of W stands for branch of Lambert W function.

When considering the velocity profile of a nozzle flow, various scenarios can be distinguished based on the Mach number parameter (v_m) and the branch (k) used in the expression for the Mach number distribution, denoted as $v_0(z)$. These parameters play a crucial role in determining the flow characteristics. The selection of appropriate v_m and k values facilitates the control of the flow characteristics in the nozzle, allowing for the realization of various flow regimes, such as subsonic, supersonic, transonic, accelerating, or decelerating profiles. Different velocity profiles are shown in Fig. 2.4.

- Subsonic profile: when $v_m < 1$ and $k = 0$, the resulting velocity profile is classified as subsonic. This means that both at the entrance and exit of the nozzle, the velocity remains subsonic, and the midpoint velocity is also less than unity $(v_m < 1)$. A subsonic flow is characterized by fluid velocities that are slower than the local speed of sound. The blue and orange curves on Fig. 2.4 are both subsonic profiles. As z goes from -1 to 0, the point (z, W) moves towards the point $(-1/e, 1)$ along the $k = -1$ branch. As z goes from 0 to 1, the point (z, W) moves away $(-1/e, 1)$ along the same $k = -1$ branch.

- Supersonic profile: when $v_m > 1$ and $k = -1$, the velocity profile corresponds to a supersonic flow. In this situation, the fluid velocities at both the entrance and exit of the nozzle are supersonic, and the midpoint velocity (v_m) exceeds the value of unity $(v_m > 1)$. Supersonic flow is characterized by velocities that surpass the speed of sound. The purple and brown curves on Fig. 2.4 are both supersonic profiles. As z goes from -1 to 0, the point (z, W) moves towards the point $(-1/e, 1)$ along the $k = 0$ branch. As z goes from 0 to 1, the point (z, W) moves away $(-1/e, 1)$ along the same $k = 0$ branch.

- Accelerating profile: when $v_m = 1$, the velocity profile becomes transonic. In this case, the midpoint velocity is exactly at the sonic threshold $(v_m = 1)$, where the fluid velocity equals the local speed of sound. To achieve an accelerating velocity profile, a configuration with $k = 0$ for $z < 0$ and $k = -1$ for $z > 0$ is employed. Here, z represents the spatial coordinate along the nozzle length. With this setup, the flow starts subsonically and gradually accelerates to a supersonic speed as it propagates along the nozzle. The green curve on Fig. 2.4 is the accelerating profile. As z goes from

-1 to 0, the point (z, W) moves towards the point $(-1/e, 1)$ along the $k = -1$ branch. As z goes from 0 to 1, the point (z, W) moves away $(-1/e, 1)$ along another branch, $k = 0$.

- Decelerating profile: set $v_m = 1$ again, then a decelerating velocity profile can be obtained by adopting a similar approach but with reversed values of k. Specifically, the configuration will have $k = -1$ for $z < 0$ and $k = 0$ for $z > 0$, causing the flow to start supersonically and decelerate to subsonic velocities further down the nozzle. The red curve on Fig. 2.4 is the decelerating profile. As z goes from -1 to 0, the point (z, W) moves towards the point $(-1/e, 1)$ along the $k = 0$ branch. As z goes from 0 to 1, the point (z, W) moves away $(-1/e, 1)$ along another branch, $k = -1$.
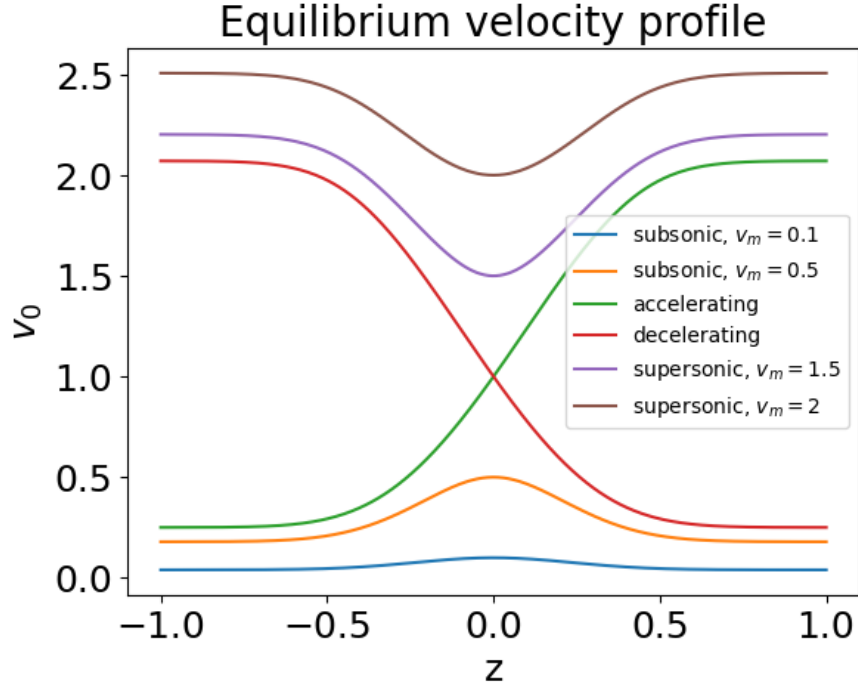
Figure 2.4: The velocity profile in the magnetic nozzle is completely determined by the midpoint mach number v_m and the branch k. A subsonic profile can be obtained by selecting $v_m < 1$ and $k = 0$. On the other hand, a supersonic profile can be obtained by setting $v_m > 1$ and $k = -1$. Lastly, for the transonic velocity profiles, the midpoint velocity is set to unity, $v_m = 1$, and then by choose $k = 0$ for $x < 0$ and $k = -1$ for $x > 0$ we get accelerating profile. Decelerating profile can be obtained similarly.

2.4 Linearized Governing Equations

As illustrated in Sec.1.2, it is essential to linearize the governing equations in order to investigate the linear instability of plasma. Now we are going to derive the linearized governing equations with the equilibrium conditions given in above.

Let $n = n_0(z) + \tilde{n}(z,t)$ and $v = v_0(z) + \tilde{v}(z,t)$, where $\tilde{n}$ and $\tilde{v}$ are small perturbed quantities.

We first linearize Eq. (2.26) by setting $n = n_0 + \tilde{n}$ and $v = v_0 + \tilde{v}$,

$$\frac{\partial(n_0 + \tilde{n})}{\partial t} + (n_0 + \tilde{n})\frac{\partial(v_0 + \tilde{v})}{\partial z} + (v_0 + \tilde{v})\frac{\partial(n_0 + \tilde{n})}{\partial z} - (n_0 + \tilde{n})(v_0 + \tilde{v})\frac{\partial_z B}{B} = 0$$

By ignoring the nonlinear terms, we obtain

$$\frac{1}{n_0}\frac{\partial\tilde{n}}{\partial t} + \frac{\partial v_0}{\partial z} + \frac{\tilde{n}}{n_0}\frac{\partial v_0}{\partial z} + \frac{\partial\tilde{v}}{\partial z} + \frac{v_0}{n_0}\frac{\partial n_0}{\partial z} + \frac{\tilde{v}}{n_0}\frac{\partial n_0}{\partial z} + \frac{v_0}{n_0}\frac{\partial\tilde{n}}{\partial z} - v_0\frac{\partial_z B}{B} - \tilde{v}\frac{\partial_z B}{B} - \tilde{n}\frac{v_0}{n_0}\frac{\partial_z B}{B} = 0$$

Using the equilibrium condition Eq. (2.28), $\partial_z v_0 + v_0\partial_z n_0/n_0$ cancels $-v_0\partial_z B/B$,

$$\frac{1}{n_0}\frac{\partial\tilde{n}}{\partial t} + \frac{\tilde{n}}{n_0}\frac{\partial v_0}{\partial z} + \frac{\partial\tilde{v}}{\partial z} + \frac{\tilde{v}}{n_0}\frac{\partial n_0}{\partial z} + \frac{v_0}{n_0}\frac{\partial\tilde{n}}{\partial z} - \tilde{v}\frac{\partial_z B}{B} - \tilde{n}\frac{v_0}{n_0}\frac{\partial_z B}{B} = 0$$

Moreover, the last term can be written as

$$\tilde{n}\frac{v_0}{n_0}\frac{\partial_z B}{B} = \frac{\tilde{n}}{n_0}\left(\frac{\partial_z n_0}{n_0}v_0 + \frac{\partial v_0}{\partial z}\right)$$

Now, we get the linearized conservation of mass,

$$\frac{1}{n_0}\frac{\partial\tilde{n}}{\partial t} + \frac{\partial\tilde{v}}{\partial z} + v_0\tilde{Y} + \tilde{v}\frac{\partial_z n_0}{n_0} - \tilde{v}\frac{\partial_z B}{B} = 0 \tag{2.33}$$

where

$$\tilde{Y} \equiv \frac{1}{n_0}\frac{\partial\tilde{n}}{\partial z} - \frac{\partial_z n_0}{n_0^2}\tilde{n} = \frac{\partial}{\partial z}\left(\frac{\tilde{n}}{n_0}\right)$$

To linearize the conservation of momentum, we follow the same logic by substituting $n = n_0 + \tilde{n}$, and $v = v_0 + \tilde{v}$ in Eq. (2.27),

$$(n_0 + \tilde{n})\frac{\partial(v_0 + \tilde{v})}{\partial t} + (n_0 + \tilde{n})(v_0 + \tilde{v})\frac{\partial(v_0 + \tilde{v})}{\partial z} = -\frac{\partial(n_0 + \tilde{n})}{\partial z}$$

Again, ignore second order perturbations and rearrange terms, we have

$$\frac{\partial \tilde{v}}{\partial t} + v_0 \frac{\partial \tilde{v}}{\partial z} + \tilde{v} \frac{\partial v_0}{\partial z} = -\frac{1}{n_0} \frac{\partial n_0}{\partial z} - \frac{1}{n_0} \frac{\partial \tilde{n}}{\partial z} - v_0 \frac{\partial v_0}{\partial z} - \frac{\tilde{n}}{n_0} v_0 \frac{\partial v_0}{\partial z}$$

Using the equilibrium condition Eq. (2.29) on the RHS, we get the linearized conservation of momentum,

$$\frac{\partial \tilde{v}}{\partial t} + \frac{\partial (v_0 \tilde{v})}{\partial z} = -\tilde{Y} \tag{2.34}$$

2.5 Polynomial Eigenvalue Problem

We can further simplify the problem by combining Eq. (2.33) and Eq. (2.34) into a single equation. We can substitute Eq. (2.34) into Eq. (2.33) to eliminate $\tilde{Y}$,

$$\frac{\partial}{\partial t} \frac{\tilde{n}}{n_0} + \frac{\partial \tilde{v}}{\partial z} - v_0 \left(\frac{\partial}{\partial t} \tilde{v} + \frac{\partial (v_0 \tilde{v})}{\partial z} \right) + \tilde{v} \frac{\partial_z n_0}{n_0} - \tilde{v} \frac{\partial_z B}{B} = 0 \tag{2.35}$$

In order to investigate the linear instability of the flow, we need to formulate it as an eigenvalue problem. To do that, we assume the perturbed density and velocity are oscillatory, i.e. $\tilde{n}, \tilde{v} \sim \exp(-i\omega t)$, where ω is the oscillation frequency of the perturbed quantities. This frequency can be a complex number.

As illustrated in Sec.1.2, the flow can be stable or unstable depending on the imaginary part of the frequency. If $\text{Im}(\omega) > 0$, then the perturbed quantities $\tilde{n} \sim \exp(\text{Im}(\omega)t)$, which means it grows exponentially with time, hence unstable. If $\text{Im}(\omega) \leq 0$, then the amplitude of the perturbed quantities are either unchanged or exponentially decreasing, hence the flow is stable.

By assuming oscillatory perturbed quantities, Eq. (2.35) becomes,

$$-i\omega \frac{\tilde{n}}{n_0} + \frac{\partial \tilde{v}}{\partial z} - v_0 \left(-i\omega \tilde{v} + \frac{\partial (v_0 \tilde{v})}{\partial z} \right) + \tilde{v} \frac{\partial_z n_0}{n_0} - \tilde{v} \frac{\partial_z B}{B} = 0 \tag{2.36}$$

Using the equilibrium condition Eq. (2.28), we can eliminate the term $\partial_z B/B$,

$$-i\omega \frac{\tilde{n}}{n_0} + \frac{\partial \tilde{v}}{\partial z} + v_0 \left(i\omega \tilde{v} - v_0 \frac{\partial \tilde{v}}{\partial z} - \tilde{v} \frac{\partial v_0}{\partial z} \right) - \tilde{v} \frac{\partial_z v_0}{v_0} = 0$$

Rearrange terms, we have

$$-i\omega \frac{\tilde{n}}{n_0} + i\omega v_0 \tilde{v} + (1 - v_0^2) \frac{\partial \tilde{v}}{\partial z} - \left(v_0 + \frac{1}{v_0} \right) \frac{\partial v_0}{\partial z} \tilde{v} = 0 \tag{2.37}$$

Now we take $\partial/\partial t$ on Eq. (2.34). Recall the fact that $\tilde{Y} = \partial_z(\tilde{n}/n_0)$, we have

$$\omega^2 \tilde{v} + i\omega \left(v_0 \frac{\partial \tilde{v}}{\partial z} + \tilde{v} \frac{\partial v_0}{\partial z} \right) = \frac{\partial}{\partial t} \frac{\partial}{\partial z} \left(\frac{\tilde{n}}{n_0} \right)$$

Switch the order of ∂_t and ∂_z, and recall $-i\omega\tilde{n}/n_0$ can be obtained from Eq. (2.37), we get

$$\omega^2 \tilde{v} + i\omega \left(v_0 \frac{\partial \tilde{v}}{\partial z} + \tilde{v} \frac{\partial v_0}{\partial z} \right) = \frac{\partial}{\partial z} \left(-i\omega v_0 \tilde{v} - (1 - v_0^2) \frac{\partial \tilde{v}}{\partial z} + \left(v_0 + \frac{1}{v_0} \right) \frac{\partial v_0}{\partial z} \tilde{v} \right)$$

Expand the RHS and collect terms, we get

$$\omega^2 \tilde{v}$$

$$+ 2i\omega \left(v_0 \frac{\partial}{\partial z} + \frac{\partial v_0}{\partial z} \right) \tilde{v}$$

$$+ \left[(1 - v_0^2) \frac{\partial^2}{\partial z^2} - \left(3v_0 + \frac{1}{v_0} \right) \frac{\partial v_0}{\partial z} \frac{\partial}{\partial z} - \left(1 - \frac{1}{v_0^2} \right) \left(\frac{\partial v_0}{\partial z} \right)^2 - \left(v_0 + \frac{1}{v_0} \right) \frac{\partial^2 v_0}{\partial z^2} \right] \tilde{v} = 0$$

(2.38)

In mathematical terms, Eq. (2.38) is a polynomial eigenvalue problem, where ω is an eigenvalue to the problem, and the velocity perturbation $\tilde{v}$ is an eigenfunction associated with the eigenvalue ω. In the later chapters we will discuss the methods to tackle this problem.

2.6 Analytical Solutions to Constant Velocity Case

In this section we are going to tackle the simplest case of the polynomial eigenvalue problem, Eq. (2.38), the constant velocity case.

The constant velocity profile can be viewed as the limit of $v_0(z)$ as the spread of magnetic field goes to infinity, $\delta \to \infty$. As the parameter δ approaches infinity, the width of the magnetic field enlarges and eventually becomes flat. In other words, a constant magnetic field. We can easily see that the velocity profile $v_0(z)$ becomes a constant as well.

If we set the velocity profile of the equilibrium flow to constant $v_0 = \mathrm{const}$, then Eq. (2.38) becomes a simple boundary value problem with second order constant coefficients differential equation.

$$\omega^2 \tilde{v} + 2i\omega v_0 \frac{\partial \tilde{v}}{\partial z} + (1 - v_0^2) \frac{\partial^2 \tilde{v}}{\partial z^2} = 0 \tag{2.39}$$

We need two boundary values in order to uniquely determine the solution (up to a constant). In the following subsections, we will solve Eq. (2.38) with constant velocity under

two sets of boundary conditions, Dirichlet and fixed-open boundary condition.

2.6.1 Dirichlet Boundary

In this subsection, the so-called Dirichlet boundary condition will be used. It has the name because the function values are fixed at the two ends of the nozzle,

$$\tilde{v}(-1) = \tilde{v}(1) = 0 \tag{2.40}$$

At the left end (entrance of the nozzle), $z = -1$, we assume there are no perturbations. As for the right end (exit of the nozzle), $z = 1$, setting the velocity perturbation to 0 might not be the best boundary condition to describe the physical process of the plasma flow in the nozzle, it nevertheless serves as a starting point to the problem and is also useful to test numerical solutions.

With the two boundary conditions, the solution to the second order constant coefficients differential equation Eq. (2.39) will be a linear combination of terms of the form $e^{ik(z+1)}$,

$$\tilde{v}(z) = C \left[\exp\left(i\omega \frac{z+1}{v_0+1} \right) - \exp\left(i\omega \frac{z+1}{v_0-1} \right) \right] \tag{2.41}$$

where $C \in \mathbb{C}$ is a complex constant, and the frequencies (eigenvalues) are

$$\omega_n = n\pi(1 - v_0^2)/2, \quad n \in \mathbb{Z} \tag{2.42}$$

The results are plotted in Fig. 2.5 This result tells us that the flow in a magnetic nozzle with uniform magnetic field is stable regardless the velocity v_0 for constant velocity case.

This solution is exact, we will use this to benchmark the simulation results in later chapter.
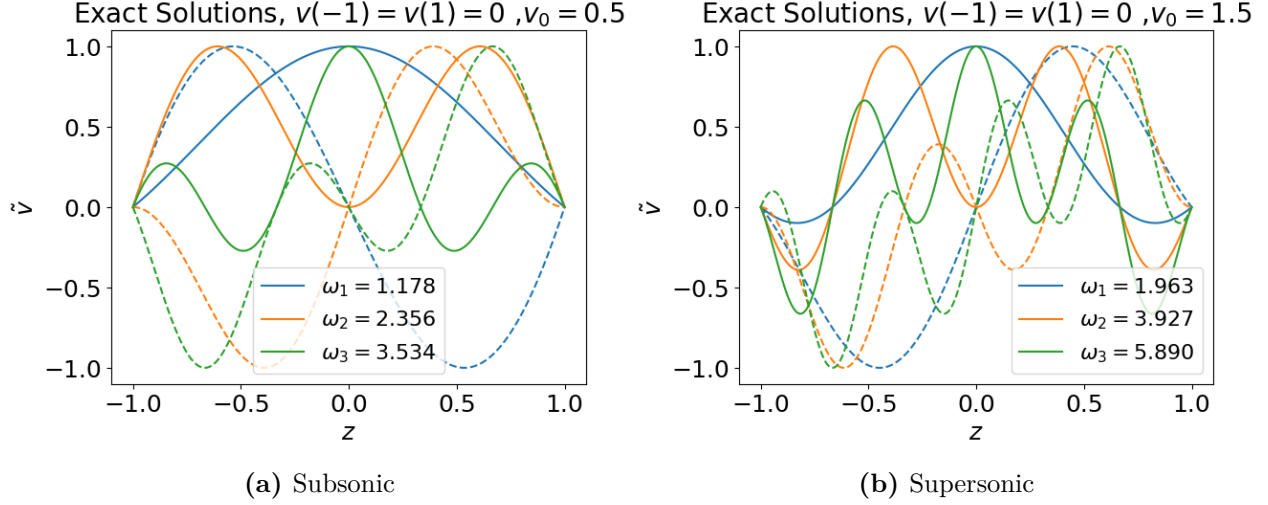
2.6.2 Fixed-Open Boundary

Fixed-Open boundary condition assumes that there are no perturbations at the entrance of the nozzle, and it is free on the exit of the nozzle.

$$\omega^2 \tilde{v} + 2i\omega v_0 \frac{\partial \tilde{v}}{\partial z} + (1 - v_0^2) \frac{\partial^2 \tilde{v}}{\partial z^2} = 0 \quad \tilde{v}(-1) = \frac{\partial \tilde{v}}{\partial z}(1) = 0 \tag{2.43}$$

The solution to this problem is similar to Eq. (2.41), the only difference is the eigenvalues. In this case, the eigenvalues are

$$\omega_n = (v_0^2 - 1) \left[\frac{n\pi}{2} - \frac{1}{4} i \ln\left(\frac{v_0-1}{v_0+1} \right) \right], \quad n \in \mathbb{Z} \tag{2.44}$$
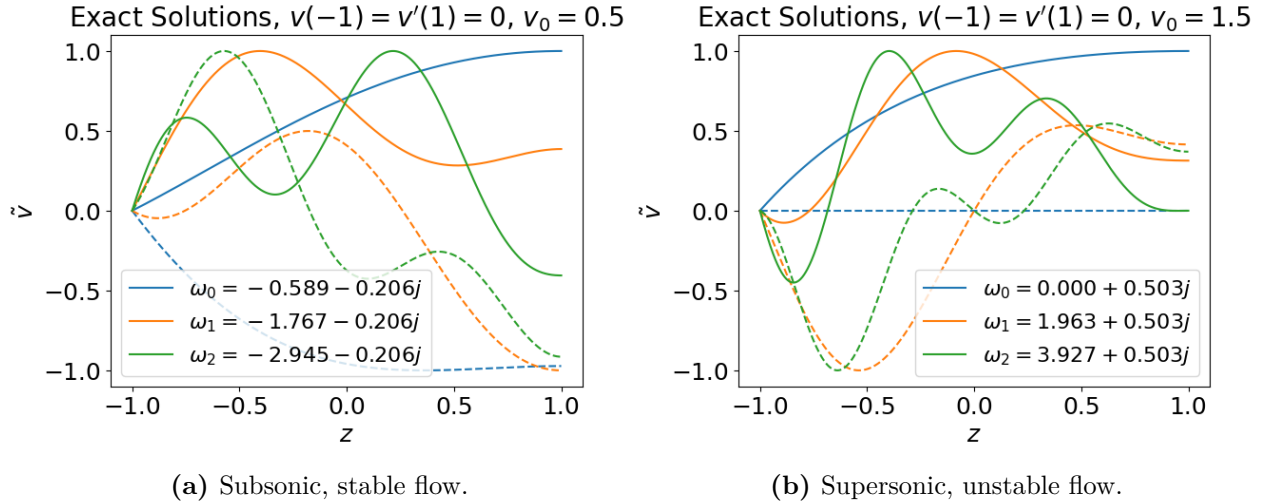
(a) Subsonic

(b) Supersonic

Figure 2.5: The plots show the first three non-zero exact solutions to Eq. (2.39) for both subsonic and supersonic case. These solutions are stable.

The growth rate is independent of the mode number n, and it is always $\ln((v_0 - 1)/(v_0 + 1))$. It is is positive for any $v_0 \neq 1$. Therefore,

- If $v_0 < 1$, then $\text{Im}(\omega) < 0$, it's damped oscillation, hence stable.

- If $v_0 > 1$, then $\text{Im}(\omega) > 0$, it's unstable.

(a) Subsonic, stable flow.

(b) Supersonic, unstable flow.

Figure 2.6: The plots show the first three exact solutions to Eq. (2.43) for both subsonic and supersonic case. The flow is stable for subsonic case and unstable for supersonic case.

Chapter 3

Spectral Method

Spectral method is an important tool for solving problems related to partial differential equations. It can provide superior accuracy compare to other local methods such as finite difference. [30] In this thesis, we are going to solve a polynomial eigenvalue problem, i.e. Eq. (2.38) together with specific boundary conditions.

Suppose the velocity perturbation $\tilde{v}$ can be approximated by some orthogonal basis functions $\{u_k(z)\}_{k=1}^{\infty}$ on $-1 \leq z \leq 1$,

$$\tilde{v} = \sum_{k=0}^{N} c_k u_k(z) \tag{3.1}$$

where c_k are coefficients to be determined. There are different choices for $u_k(z)$ including but not limited to, [30]

- $u_k(z) = T_k(z)$ (Chebyshev spectral method)

- $u_k(z) = L_k(z)$ (Legendre spectral method)

- $u_k(z) = H_k(z)$ (Hermite spectral method)

where T_k, L_k and H_k are Chebyshev, Legendre, and Hermite polynomials of degree k.

Using the above approximation in Eq. (2.38), and take the inner product with some other test functions $\{\psi_k(z)\}$ on $[-1, 1]$, the left-hand side of Eq. (2.38) becomes a matrix equation,

$$(\omega^2 \mathbf{1} + \omega \mathbf{M} + \mathbf{N})\mathbf{c} = \mathbf{0} \tag{3.2}$$

where $\mathbf{c} = [c_0, \cdots, c_N]^T$ is a vector of coefficients, and

$$M_{jk} = 2i \int_{-1}^{1} dz \; \psi_j \left(v_0 \frac{\partial}{\partial z} + \frac{\partial v_0}{\partial z} \right) u_k \tag{3.3}$$

$$N_{jk} = \int_{-1}^{1} dz \; \psi_j \left[(1 - v_0^2) \frac{\partial^2}{\partial z^2} - \left(3v_0 + \frac{1}{v_0} \right) \frac{\partial v_0}{\partial z} \frac{\partial}{\partial z} - \left(1 - \frac{1}{v_0^2} \right) \left(\frac{\partial v_0}{\partial z} \right)^2 - \left(v_0 + \frac{1}{v_0} \right) \frac{\partial^2 v_0}{\partial z^2} \right] u_k \tag{3.4}$$

Depending on the choice of the test function, spectral method can be further classified, [30]

- Galerkin: The test functions are the same as the trial ones, i.e. $\psi_k = u_k$.

- Collocation: The test functions $\{\psi_k\}$ are Lagrange basis polynomials such that $\psi_k(z_j) = \delta_{jk}$, where z_j are preassigned collocation points.

To solve Eq. (3.2), we simply augment the coefficient vector to $[\mathbf{c}, \omega\mathbf{c}]^T$. Then the matrix equation can be written as an algebraic eigenvalue problem,

$$\begin{bmatrix} \mathbf{0} & \mathbf{1} \\ -\mathbf{N} & -\mathbf{M} \end{bmatrix} \begin{bmatrix} \mathbf{c} \\ \omega\mathbf{c} \end{bmatrix} = \omega \begin{bmatrix} \mathbf{c} \\ \omega\mathbf{c} \end{bmatrix} \tag{3.5}$$

We can apply standard eigenvalue problem solver to this question to obtain the eigenvalues ω and their corresponding eigenvectors $[\mathbf{c}, \omega\mathbf{c}]^T$. Therefore, the eigenfunctions $\tilde{v} = \sum_k c_k u_k(z)$ to the original problem can be recovered by extracting coefficients $\mathbf{c}$ from the eigenvectors.

3.1 Spectral Collocation Method

One of the methods we are going to use is called the Chebyshev collocation method. Given a set of Chebyshev points, $\{z_j = \cos(j\pi/N)\}_{j=0}^{N}$, and let $\{h_j\}$ be the Lagrange basis polynomials associated with $\{z_j\}_{j=0}^{N}$, and define matrix $D_{kj} = h_j'(z_k)$. By setting $\tilde{v}(z) = \sum_{j=0}^{N} c_j h_j(z)$, we see that

$$\tilde{v}(z_k) = \sum_{j=0}^{N} \tilde{v}_j h_j(z_k) = c_k \tag{3.6}$$

$$\tilde{v}'(z_k) = \sum_{j=0}^{N} \tilde{v}_j h_j'(z_k) = \sum_{j=0}^{N} D_{kj} c_j \tag{3.7}$$

$$\tilde{v}''(z_k) = \sum_{j=0}^{N} \tilde{v}_j h_j''(z_k) = \sum_{j=0}^{N} D_{kj}^2 c_j \tag{3.8}$$

We see that the coefficient vector **c** becomes a vector containing the values of $\tilde{v}$ evaluated at the collocation points, i.e. $\mathbf{c} = [v(z_0), \cdots, v(z_N)]^T$, and the matrix D and D^2 act as the differential operators $\frac{\partial}{\partial z}$ and $\frac{\partial^2}{\partial z^2}$, respectively. The matrix D is called Chebyshev differentiation matrix since it acts as $\frac{\partial}{\partial z}$ and evaluates at Chebyshev points.

Chebyshev Differentiation Matrix

The Chebyshev differentiation matrix finds the derivative of the Lagrange interpolant of the given data points $(z_j, \tilde{v}(z_j))$ where $\{z_j = \cos(j\pi/N)\}_{j=0}^N$ are the Chebyshev points. Suppose $\mathbf{v} = [v(z_0), \cdots, v(z_N)]^T$, then the N-point, D_N, Chebyshev differentiation matrix gives $D_N \mathbf{v} \approx [v'(z_0), \cdots, v'(z_N)]^T$. Higher order differentiation can be achieved by taking powers of D_N. Thanks to [35], the construction of Chebyshev differentiation matrix is given in Fig. 3.1.

If we instead use the equal-spaced points, $\{z_j = 2j/N\}_{j=0}^N$, then the matrix defined by $D_{kj} = h_j'(x_k)$ will be the usual finite difference differentiation matrix. However, Chebyshev differentiation matrix has superior accuracy due to the wise choice of collocation points. On Fig. 3.2 we see that the Chebyshev achieve higher accuracy.

Dirichlet Boundary

To implement Dirichlet boundary condition, $\tilde{v}(\pm 1) = 0$, to Eq. (3.2), we only need to remove the first and last columns and rows of each matrix, $\mathbf{0}, \mathbf{1}, \mathbf{M}$, and $\mathbf{N}$. The reason is originated from the Chebyshev differentiation matrix, Fig. 3.3. For a $(N+1) \times (N+1)$ Chebyshev differentiation matrix D_N, the first and last row has no effect since the first and last value of $\tilde{v}$ are 0. We only need the interior of D_N which is an $N \times N$ matrix. After solving Eq. (3.2), we get the eigenvalues ω and their associated eigenfunctions evaluated at the interior collocation points $\mathbf{c} = [\tilde{v}_1, \cdots, \tilde{v}_{N-1}]^T$. We will need to prepend and append 0 to the eigenfunctions, $[0, \tilde{v}_1, \cdots \tilde{v}_{N-1}, 0]^T$. Listing. 3.1 has the pseudocode for solving Eq. (3.2).

Fixed-Open Boundary

To implement fixed-open boundary condition, i.e. $\tilde{v}(-1) = \tilde{v}'(1) = 0$. Notice that $\tilde{v}'(-1)$ can be expressed as,

$$0 = \tilde{v}'(1) = \sum_{j=0}^N D_{ij} \tilde{v}_j \tag{3.9}$$

$$
D_N = \begin{array}{|c|c|c|}
\hline
\dfrac{2N^2+1}{6} & 2\dfrac{(-1)^j}{1-x_j} & \dfrac{1}{2}(-1)^N \\
\hline
-\dfrac{1}{2}\dfrac{(-1)^i}{1-x_i} & \begin{array}{c} \dfrac{(-1)^{i+j}}{x_i-x_j} \\[2mm] \dfrac{-x_j}{2(1-x_j^2)} \\[2mm] \dfrac{(-1)^{i+j}}{x_i-x_j} \end{array} & \dfrac{1}{2}\dfrac{(-1)^i}{1+x_i} \\
\hline
-\dfrac{1}{2}(-1)^N & -2\dfrac{(-1)^{N+j}}{1-x_j} & -\dfrac{2N^2+1}{6} \\
\hline
\end{array}
$$

Figure 3.1: Construction of N-point Chebyshev differentiation matrix. The nodes $x_j = \cos(j\pi/N)$ are Chebyshev points. Adapted from [35].

```python
import numpy as np
# collocation points, differentiation matrices
N = 101 # number of points
x, D1, D2 = Chebyshev(N)
# solve polynomial eigenvalue problem
A11 = np.zeros_like(D1)
A12 = np.eye(*D1.shape)
A21 = -np.diag(1-v0**2)@D2 \
        + np.diag((3*v0 + 1/v0)*(D1@v0))@D1 \
        + np.diag((1-1/v0**2)*(D1@v0)**2) \
        + np.diag((v0+1/v0)*(D2@v0))
A22 = -2j*(np.diag(v0)@D1 + np.diag(D1@v0))
A = np.block([[A11[1:-1,1:-1], A12[1:-1,1:-1]],
              [A21[1:-1,1:-1], A22[1:-1,1:-1]]])
omega, V = np.linalg.eig(A)
# pad two ends of eigenfunctions by 0 (dirichlet boundary)
V = np.pad(V,((1,1),(0,0)))
```

Listing 3.1: Pseudocode for solving polynomial eigenvalue problem using spectral collocation with Dirichlet boundary condition.
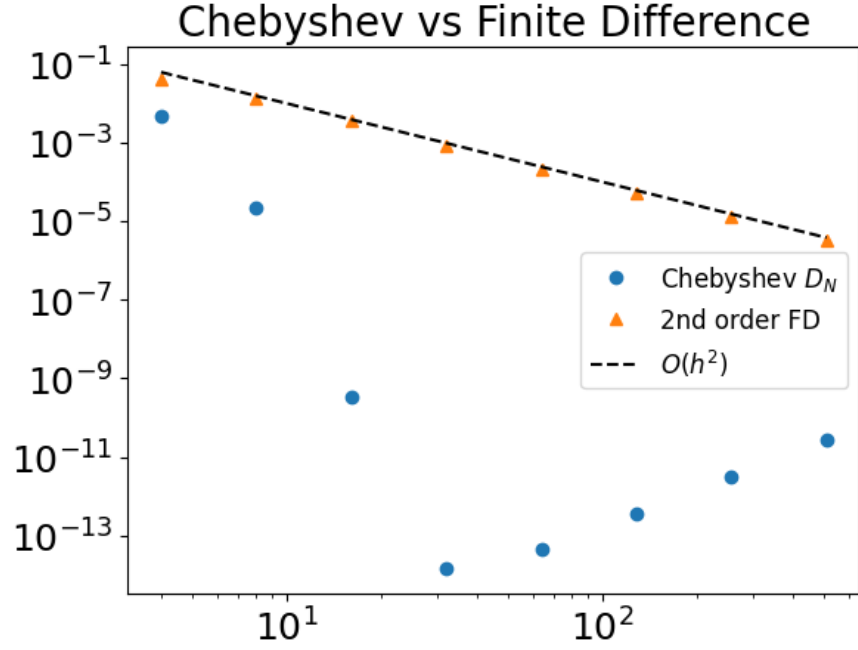
Figure 3.2: Comparison of accuracy between Chebyshev differentiation matrix and 2nd order finite difference differentiation matrix. Both methods are applied to compute the derivative of function $f(x) = \ln(2 + \sin(x))$ on $[-1, 1]$. Chebyshev differentiation achieve higher accuracy and converge faster than finite difference.

Figure 3.3: Since the function v is zero at x_0 and x_N, the first and last columns has no effect and the same argument applies to first and last rows. Adapted from [35].

where $\tilde{v}_j = \tilde{v}(z_j)$ is the evaluation of $\tilde{v}$ at Chebyshev points $z_j = \cos(j\pi/N)$. By rearranging the terms, we get the expression of $\tilde{v}_0$ in terms of $\tilde{v}$ at other collocation points.

$$\tilde{v}_0 = -\frac{1}{D_{00}} \sum_{j=1}^{N} D_{0j}\tilde{v}_j \tag{3.10}$$

To incorporate this information into the differentiation matrix, we modify the expressions for evaluating the derivatives at point x_1,

$$\tilde{v}_1' = \sum_{j=0}^{N} D_{1j}\tilde{v}_j = \sum_{j=1}^{N} \left(D_{1j} - \frac{D_{10}}{D_{00}} D_{0j} \right) \tilde{v}_j \tag{3.11}$$

$$\tilde{v}_1'' = \sum_{j=0}^{N} D_{1j}^2 \tilde{v}_j = \sum_{j=1}^{N} \left(D_{1j}^2 - \frac{D_{10}^2}{D_{00}} D_{0j} \right) \tilde{v}_j \tag{3.12}$$

This indicates the new differentiation matrices should be

$$D_{ij}' = \begin{cases} D_{ij}, & \text{if } i \neq 1 \\ D_{1j} - \frac{D_{10}}{D_{00}} D_{0j}, & \text{if } i = 1 \end{cases} \tag{3.13}$$

$$D_{ij}'^2 = \begin{cases} D_{ij}^2, & \text{if } i \neq 1 \\ D_{1j}^2 - \frac{D_{10}^2}{D_{00}} D_{0j}, & \text{if } i = 1 \end{cases} \tag{3.14}$$

After getting the eigenfunctions $\mathbf{c} = [\tilde{v}_1, \cdots, \tilde{v}_N]^T$, we need to prepend $\tilde{v}_0$ to $\mathbf{c}$ using Eq. (3.10). See Listing. 3.2 for pseudocode.

3.2 Spectral Galerkin Method

Another spectral method we used in the numerical experiments is the Legendre-Galerkin method. Meaning that the basis functions are chosen to be the compact combinations of Legendre polynomials, [30]

$$u_k(z) = L_k(z) + a_k L_{k+1}(z) + b_k L_{k+2}(z) \tag{3.15}$$

where the parameters $\{a_k, b_k\}$ are chosen to satisfy the boundary conditions. The test functions are the same as the basis functions.

Suppose the boundary conditions are

$$a_- \tilde{v}(-1) + b_- \tilde{v}'(-1) = 0, \, a_+ \tilde{v}(1) + b_+ \tilde{v}'(1) = 0$$

```
1  import numpy as np
2  # collocation points, differentiation matrices
3  N = 101 # number of points
4  x, D1, D2 = Chebyshev(N)
5  # modify second row to ensure v'(1)=0
6  D1v = D1
7  D2v = D2
8  D1v[1,:] = D1[1,:] - D1[1,0]/D1[0,0]*D1[0,:]
9  D2v[1,:] = D2[1,:] - D2[1,0]/D1[0,0]*D1[0,:]
10 # only the differential operators acting on v needs to be modified
11 A11 = np.zeros_like(D1)
12 A12 = np.eye(*D1.shape)
13 A21 = -np.diag(1-v0**2)@D2v \
14        + np.diag((3*v0 + 1/v0)*(D1@v0))@D1v \
15        + np.diag((1-1/v0**2)*(D1@v0)**2) \
16        + np.diag((v0+1/v0)*(D2@v0))
17 A22 = -2j*(np.diag(v0)@D1v + np.diag(D1@v0))
18 A = np.block([[A11[:-1,:-1], A12[:-1,:-1]],
19               [A21[:-1,:-1], A22[:-1,:-1]]])
20 omega, V = np.linalg.eig(A)
21 # add v(1) to eigenfunctions
22 V = np.pad(V,((1,0),(0,0)))
23 for j in range(V.shape[1]):
24     V[0,j] = -(D1[0,1:]@V[1:,j])/D1[0,0]
```

Listing 3.2: Pseudocode for solving polynomial eigenvalue problem using spectral collocation with fixed-open boundary condition.

Then the parameters $\{a_k, b_k\}$ can be worked out by simple linear algebra,

$$a_k = \frac{(2k+3)(a_+ b_- + a_- b_+)}{\text{DET}_k}$$
$$b_k = \frac{-2a_- a_+ + (k+1)^2(a_+ b_- - a_- b_+) + b_- b_+ k(k+1)^2(k+2)/2}{\text{DET}_k} \quad (3.16)$$

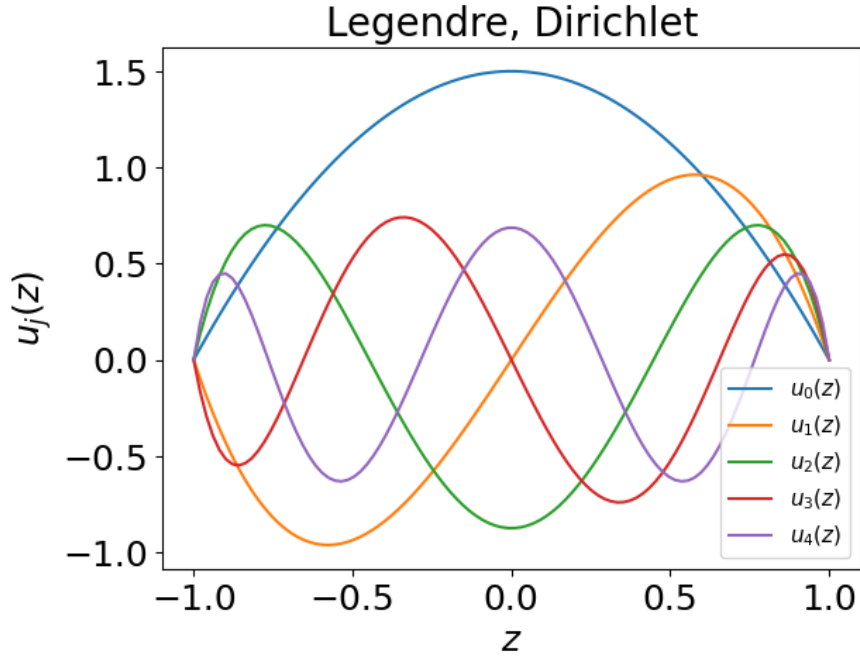where $\text{DET}_k = 2a_+ a_- + a_- b_+(k+2)^2 - a_+ b_-(k+2)^2 - b_- b_+(k+1)(k+2)^2(k+3)/2$.

Dirichlet Boundary

The necessary parameters to make $u_k(\pm 1) = 0$ are $a_k = 0, b_k = -1$. The basis functions are therefore,

$$u_k(z) = L_k(z) - L_{k+2}(z) \quad (3.17)$$
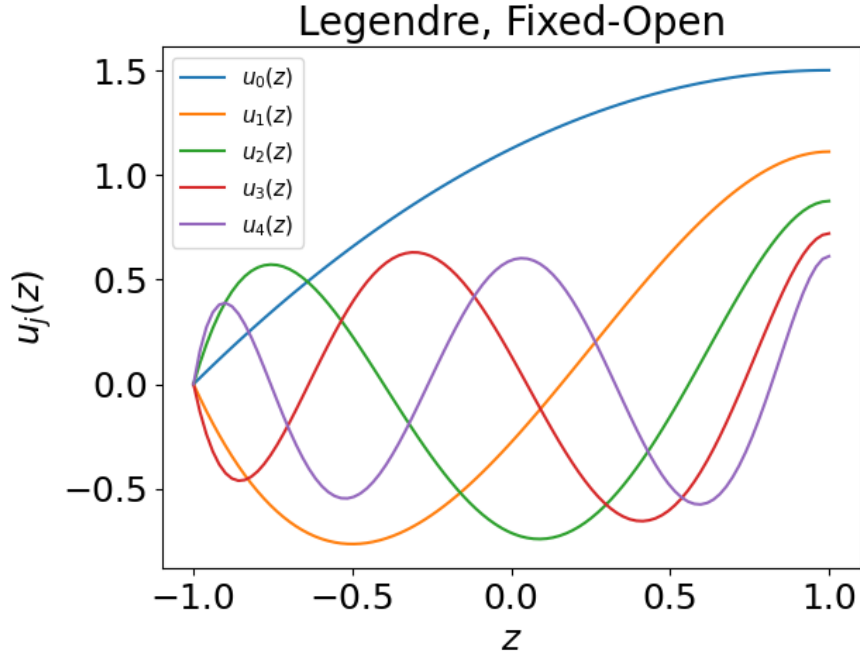
The first 5 basis functions are shown in Fig. 3.4.

Figure 3.4: Compact Legendre combinations satisfying Dirichlet boundary condition.

Fixed-Open Boundary

The necessary parameters to make $u_k(-1) = u'_k(1) = 0$ are $a_k = (2k+3)/(k+2)^2, b_k = -(k+1)^2/(k+2)^2$. The basis functions are therefore,

$$u_k(z) = L_k(z) + \frac{2k+3}{(k+2)^2}L_{k+1}(z) - \frac{(k+1)^2}{(k+2)^2}L_{k+2}(z) \tag{3.18}$$

The first 5 basis functions are shown in Fig. 3.5.

Figure 3.5: Compact Legendre combinations satisfying fixed-open boundary condition.

By setting $\tilde{v}(z) = \sum_{j=0}^{N} c_k u_k(z)$, $\tilde{v}$ satisfies the boundary conditions automatically. There is no need to modify the matrices in Eq. (3.2).

To evaluate the matrix elements, inner products are calculated by numerical integration, in this thesis Simpson's rule is used. Eq. (3.3) and Eq. (3.4) become

$$M_{jk} = 2i \sum_{m}^{M} w_m \Delta z_m \left[\psi_j \left(v_0 \frac{\partial}{\partial z} + \frac{\partial v_0}{\partial z} \right) u_k \right]_{z_m} \tag{3.19}$$

$$N_{jk} = \sum_{m}^{M} w_m \Delta z_m \left\{ \psi_j \left[(1 - v_0^2) \frac{\partial^2}{\partial z^2} - \left(3v_0 + \frac{1}{v_0} \right) \frac{\partial v_0}{\partial z} \frac{\partial}{\partial z} - \left(1 - \frac{1}{v_0^2} \right) \left(\frac{\partial v_0}{\partial z} \right)^2 - \left(v_0 + \frac{1}{v_0} \right) \frac{\partial^2 v_0}{\partial z^2} \right] u_k \right\}_z \tag{3.20}$$

```python
import numpy as np
from scipy.special import lengendre # lengendre polynomials
from scipy.integrate import simpson # simpson quadrature
# collocation points, differentiation matrices
N = 25 # number of basis functions
M = 101 # number of points
x, D1, D2 = Chebyshev(M, "symmetric", "CH")
# use this basis for drichlet boundary
u = lambda x,k: (legendre(k) + (2*k+3)/(k+2)**2*legendre(k+1) - (k+1)**2/(k+2)
    **2*legendre(k+2))(x)
# use this basis for fixed-open boundary
u = lambda x,k: (legendre(k) - legendre(k+2))(x)
# solve polynomial eigenvalue problem
A11 = np.zeros_like(D1)
A12 = np.eye(*D1.shape)
A21 = np.zeros((N,N),dtype=complex)
A22 = np.zeros((N,N),dtype=complex)
for i in range(N):
    for j in range(N):
    A21[i,j] = simpson(
      - u(x,i)*(1-v0**2)*(D2@u(x,j))
      + u(x,i)*(3*v0+1/v0)*(D1@v0)*(D1@u(x,j))
      + u(x,i)*(1-1/v0**2)*(D1@v0)**2*u(x,j)
      + u(x,i)*(v0+1/v0)*(D2@v0)*u(x,j),
      x=x)
    A22[i,j] = -2j*simpson(u(x,i)*v0*(D1@u(x,j)) + u(x,i)*(D1@v0)*u(x,j),x=x)
A = np.block([[A11, A12],
              [A21, A22]])
omega, C = np.linalg.eig(A)
# construct eigenfunctions
V = np.zeros((x.size, C.shape[1]),dtype=complex)
for i in range(C.shape[1]):
    for k in range(N):
        V[:, i] += C[k,i]*u(x, k)
```

Listing 3.3: Pseudocode for solving polynomial eigenvalue problem using Lengendre-Galerkin method

where M is the number of points, $\Delta z_m = 2/M$, and w_m are coefficients corresponding to the quadrature rule employed. In this case,

$$w_n = \begin{cases} 1/3, \text{if } m = 0, M \\ 4/3, \text{if } m \text{ is odd} \\ 2/3, \text{if } m \neq 0, M \text{ and } m \text{ is even} \end{cases} \tag{3.21}$$

After solving Eq. (3.2), the eigenvector **c** can be used to reconstruct the eigenfunctions. See Listing. 3.3 for more details.

3.3   Spectral Theory in Finite-Dimensional Normed Spaces

Spectral method transforms the polynomial eigenvalue problem to an algebraic eigenvalue problem. For completion, some important linear algebra results are included in this section.

Let X be a finite dimensional normed space and $\hat{T} : X \to X$ a linear operator. Since any linear operator can be represented by a matrix, the spectral theory of $\hat{T}$ is essentially matrix eigenvalue theory. [22] Let A be a matrix representation of $\hat{T}$, then we have the definition.

Definition 2 (Kryszig [22]). An eigenvalue of a square matrix A is a complex number λ such that

$$Ax = \lambda x$$

has a solution $x \neq 0$. This x is called an **eigenvector** of A corresponding to that eigenvalue λ. The set $\sigma(A)$ of all eigenvalues of A is called the **spectrum** of A. Its complement $\rho(A) = \mathbb{C} - \sigma(A)$ in the complex plane is called the **resolvent** set of A.

By choosing different bases in X, we can have different matrix representation of $\hat{T}$. We need to make sure the eigenvalues of a linear operator is independent of the basis chosen. Fortunately, a theorem ensures that.

Theorem 1 (Kryszig [22]). All matrices representing a given linear operator $\hat{T} : X \to X$ on a finite dimensional normed space X relative to various bases for X have the same eigenvalues.

Moreover, we don't need to worry about the existence of eigenvalues of a linear operator. The following theorem shows the existence of them.

Theorem 2 (Kryszig [22]). A linear operator on a finite dimensional complex normed space $X \neq O$ has at least one eigenvalue.

3.4   Spectral Pollution and Spurious Modes

In this section, we will discuss an important phenomenon we observe throughout the numerical experiments using spectral method. It is the phenomenon of spectral pollution. Then we will provide a method to filter these spurious modes.

Spectral pollution refers to the phenomenon which some eigenvalues are not converging to the correct value when the mesh density is increased. The wrong eigenvalues are referred as spurious modes. When solving eigenvalue problems using spectral methods with finite difference or finite element approximations, spectral pollution might occur. [25] The cause of the spectral pollution is originated from the improper discretization of the differential operators. In the following sections, we are going to take a closer look at the differential

operators in finite difference method, and reveal the occurrence of spurious modes when solving Eq. (2.39).

3.4.1 Analysis of Numerical Spectrum

In this section, we will analyze the analytical and numerical dispersion relation of the following problem,

$$\omega^2 \tilde{v} + 2i\omega v_0 \frac{\partial \tilde{v}}{\partial z} + (1 - v_0^2)\frac{\partial^2 \tilde{v}}{\partial z^2} = 0, \quad v(\pm 1) = 0$$

It is a special case, i.e. $v_0 =$constant, of a more general problem Eq. (2.38). The analytical dispersion relation can be obtained by substituting $\tilde{v} = \exp(-i\omega t + kx)$ into the above equation,

$$\omega = k(v_0 \pm 1) \tag{3.22}$$

The dispersion relation suggests that the eigenvalue ω should be real.

Now let's analyze the dispersion relation produced by finite difference. To do this we need to first understand the effect of the differential operators on function $\tilde{v}$ in finite difference. If we assume $\tilde{v} \sim \exp(ikx)$, and let $\beta \equiv kh/2$. Then in finite difference discretization scheme, the differential operators d^n/dz^n are equivalent to the following factors [25],

$$
\begin{aligned}
\frac{d^0}{dz^0} &\rightarrow G_0 = 1 \\
\frac{d^1}{dz^1} &\rightarrow G_1 = [\exp(2i\beta) - \exp(-2i\beta)]/2h = (i/h)\sin(2\beta) \\
\frac{d^2}{dz^2} &\rightarrow G_2 = [\exp(2i\beta) - 2 - \exp(-2i\beta)]/h^2 = (2/h^2)(\cos(2\beta) - 1)
\end{aligned}
\tag{3.23}
$$

Using the G-operators, Eq. (3.23), the discretized equation of Eq. (2.39) becomes

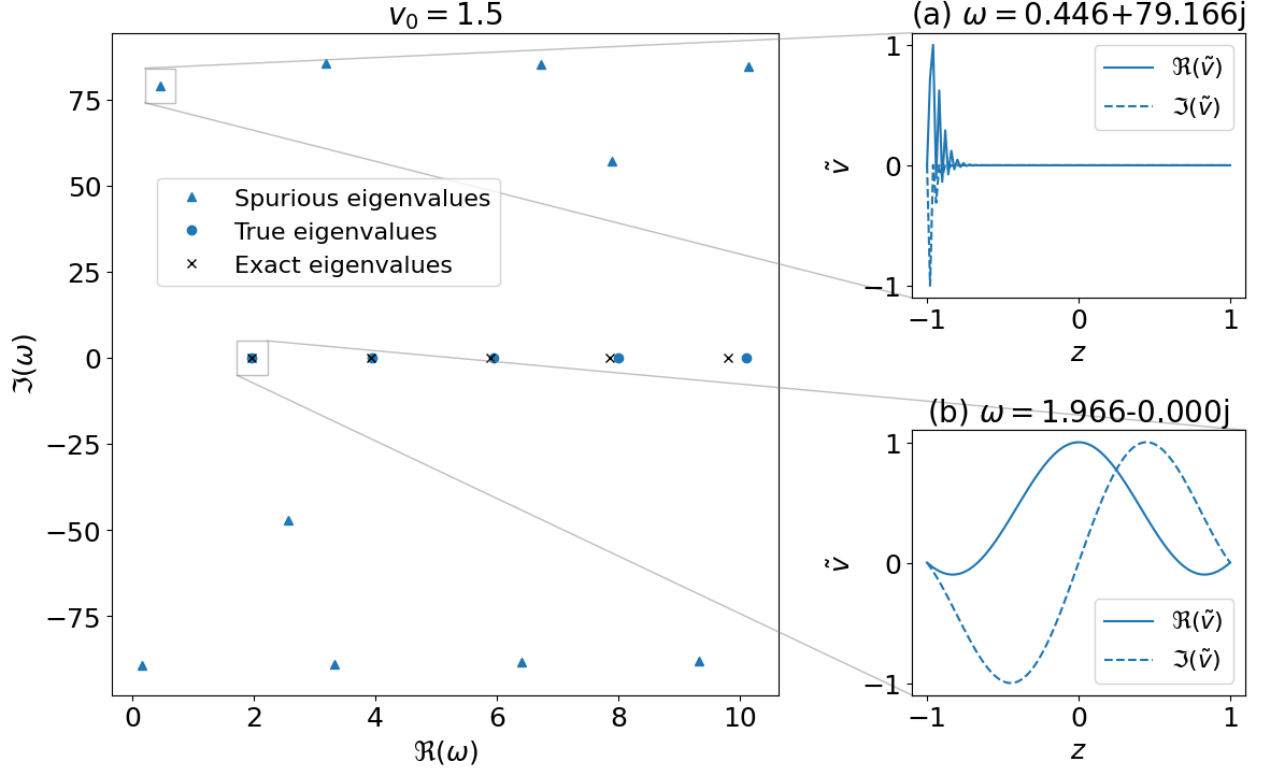$$(\omega^2 G_0 + \omega G_1 + G_2)\tilde{v} = 0 \tag{3.24}$$

Solving Eq. (3.24), we obtain the numerical dispersion relation,

$$\omega = \frac{2\sin(\beta)}{h}\left(v_0 \pm \sqrt{1 - v_0^2 \sin^2(\beta)}\right) \tag{3.25}$$

Given h (fixed the mesh resolution), we see that

- ω is real for all k if $v_0 < 1$.

- ω is complex for large k, more specifically $k > h/2\arcsin(1/v_0)$, if $v_0 > 1$.

- For small k, meaning $k \to 0$, Eq. (3.25) is a good representation for the analytical dispersion relation, Eq. (3.22).


Figure 3.6: (a) Eigenfunction corresponding to a spurious eigenvalue, the eigenfunction has weird shape. (b) Eigenfunction corresponding to a true eigenvalue.

In this simple case of solving Eq. (3.24), one way to filter the spurious modes is to remove modes with high-oscillation. That is removing modes with wave number $k > h/2 \arcsin(1/v_0)$. However, this is not possible in general cases because Eq. (3.25) is only valid if finite-difference is used, and it requires the exact solution to the discretized problem Eq. (3.24) which is not available for non-constant velocity profile.

3.4.2 Convergence Test

To filter the spurious modes is by doing a "convergence test". Since the frequency Eq. (3.25) is changing with mesh resolution h. From Fig. 3.7 we see that only the true eigenmodes converge while the eigenvalues of spurious eigenmodes changes dramatically under different resolutions. By simply solving the discretized problem using spectral method under different mesh resolution, we can pick up the true eigenmodes by observing their convergence, and filter out the spurious eigenmodes which change dramatically with varying resolution.
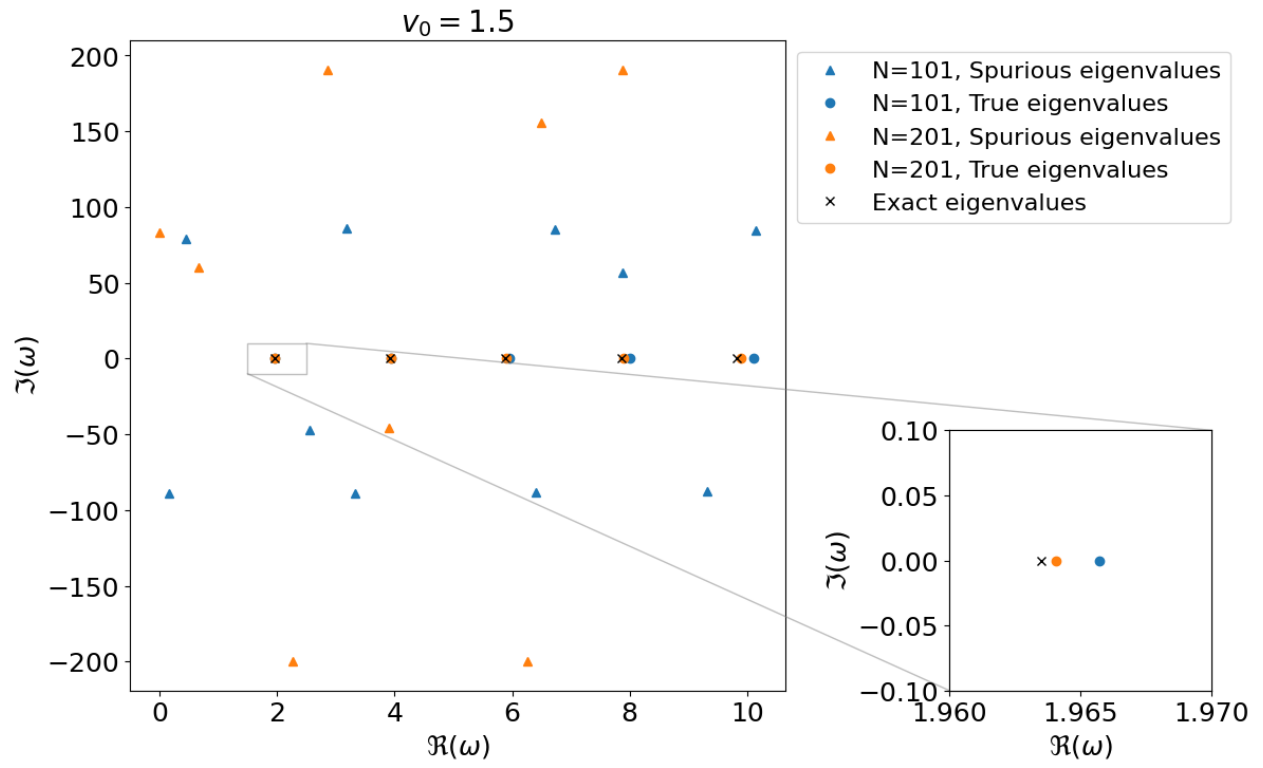
Figure 3.7: The figure shows eigenvalues under different resolutions. True eigenvalues converge to the analytical eigenvalues as resolution increases. Spurious eigenvalues diverges with no obvious pattern.

3.5 Plasma Flow with Constant Velocity Profile

In this section, we will compute the eigenmodes of the constant velocity problem with Dirichlet boundaries, Eq. (2.39), and the same problem with fixed-open boundaries, Eq. (2.43), using spectral methods. More specifically, spectral-collocation and spectral-Galerkin methods will be employed. Then spurious modes will be filtered using the convergence test prescribed in previous section. Since we have already derived the exact solutions for the constant velocity cases in Sec. 2.6, we can ensure the accuracy and reliability of the numerical methods by comparing the numerical results to the analytical ones. The parameters of spectral methods are summarized in Table. (3.1). For spectral-collocation method, we use 101 points, and for spectral-Galerkin method we use 101 points and 30 basis functions.

Table 3.1: With Dirichlet boundary condition, all methods have good accuracy, so using 101 nodes in the region $[0, 1]$ is enough. For FE and SE methods, we use 50 basis functions.

	Collocation	Galerkin
M (number of points)	101	101
N (number of basis functions)		30

3.5.1 Constant Subsonic Velocity Case

Eq. (2.39) is a special case of a more general polynomial problem Eq. (2.38). The existence of the exact solution allows us to verify the correctness of each method's implementation. This also serves as a reference to the accuracy spectral methods can achieve.

Dirichlet Boundary

Fig. 3.8 shows that the eigenvalues obtained by spectral methods agree with the theoretical eigenvalues. Table. 3.2 shows us the relative error $|\omega_{numeric} - \omega_{analytic}|/|\omega_{analytic}|$ is about 10^{-14}. Spectral methods indeed have high accuracy.

Table 3.2: Relative errors of first 5 eigenvalues obtained by spectral methods in constant subsonic velocity case with Dirichlet boundary condition. Numerical results agree with exact solution well.

| $v_0 = 0.5$	ω_1	ω_2	ω_3	ω_4	ω_5
Collocation	3.48944421e-14	6.72512513e-14	1.59603736e-14	9.81718764e-15	4.07098462e-15
Galerkin	4.09596742e-14	1.65697986e-14	4.97650778e-14	3.27344763e-13	4.11444935e-12
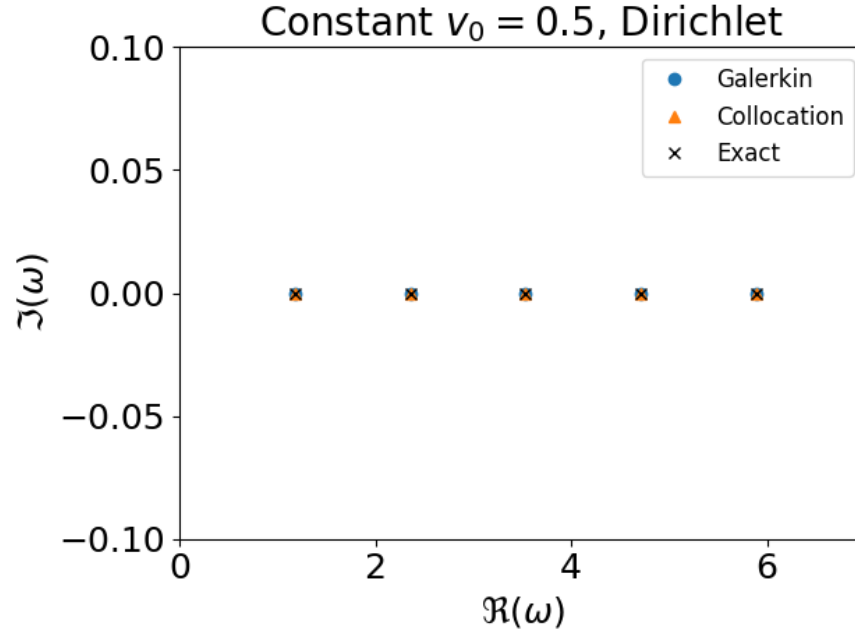
Figure 3.8: Showing the first 5 eigenvalues of each method. They are stable. Spectral methods agree with exact eigenvalues.

Fixed-Open Boundary

The numerical eigenvalues agree with the exact eigenvalues. The relative errors $|\omega_{numeric} - \omega_{analytic}|/|\omega_{analytic}|$ are about 10^{-13}. Again spectral methods has good accuracy.

Table 3.3: Relative error of each eigenvalue. Notice that the mode index starts from 0. These results agree with theory.

$v_0 = 0.5$	ω_0	ω_1	ω_2	ω_3	ω_4
Collocation	2.36006260e-12	1.95269435e-13	6.78183927e-14	2.43078107e-14	4.17011610e-14
Galerkin	2.52491323e-12	2.19414097e-13	1.82417919e-13	5.92948284e-13	4.41481039e-12
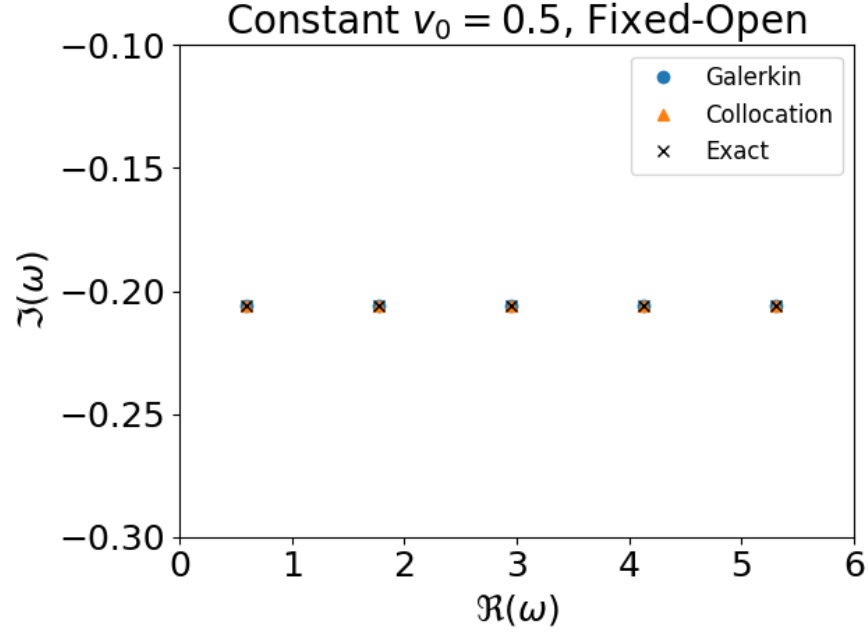
Figure 3.9: Showing the first 5 eigenvalues of each method. They are stable. The spectral methods agree with the exact eigenvalues.

### 3.5.2 Constant Supersonic Velocity Case

In supersonic case, as predicted by Sec. 3.4.1, spurious modes occur. Convergence test will be used to filter the spurious modes.

Dirichlet Boundary

In Table. 3.4, we show the first 5 filtered eigenvalues obtained by different spectral methods. It shows good agreement between the spectral methods and the theoretical eigenvalues. However, we see that the accuracy of spectral-Galerkin method drops for larger eigenvalues.

Table 3.4: Relative error of first 5 filtered eigenvalues obtained by spectral methods in constant subsonic case under Dirichlet boundary. Numerical results agree with the theory, but we see the accuracy of eigenvalues obtained from spectral-Galerkin method drops after the 3rd one.

| $v_0 = 1.5$	ω_1	ω_2	ω_3	ω_4	ω_5
Collocation	2.08984845e-13	9.29501612e-14	4.24537846e-14	3.38103217e-14	1.74476052e-14
Galerkin	1.64805562e-13	6.09485884e-14	6.81795167e-12	1.95656738e-09	1.54134402e-07

47
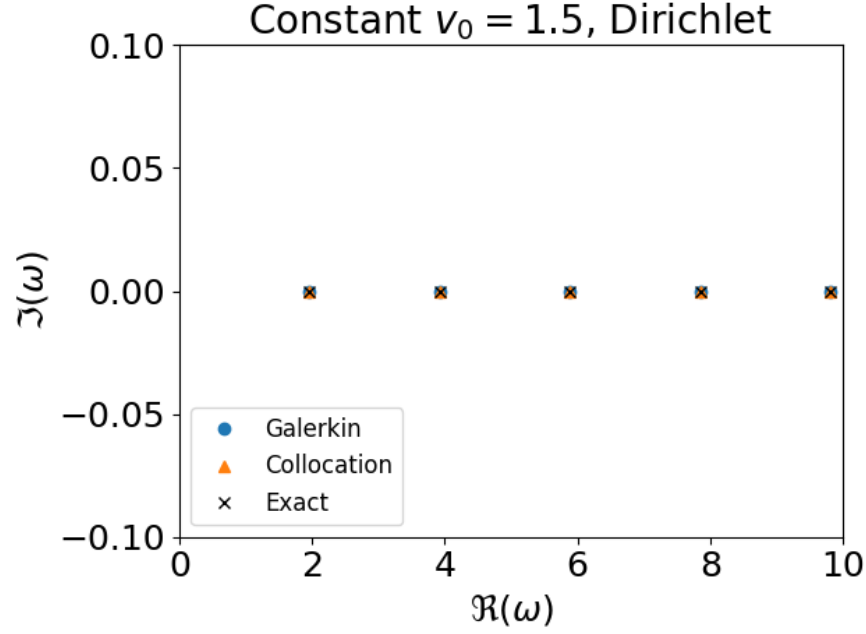
Figure 3.10: Showing the first 5 filtered eigenvalues of each method. They are stable. All methods agree with the exact eigenvalues.

Fixed-Open Boundary

Table. 3.5 shows relative error for the first 5 filtered eigenvalues obtained by different spectral methods. We see that the accuracy of spectral-Galerkin method drops for larger eigenvalues.

Table 3.5: Relative error of first 5 eigenvalues obtained by spectral methods in constant supersonic case under fixed-open boundary. Results agree with theory. The accuracy of spectral-Galerkin method drops after first few eigenvalues.

$v_0 = 1.5$	ω_0	ω_1	ω_2	ω_3	ω_4
Collocation	5.10516649e-11	3.58709292e-12	8.72529437e-13	3.24263319e-13	1.34297439e-13
Galerkin	5.38682371e-11	4.31902441e-12	1.44799870e-12	8.02395621e-11	2.05280524e-09
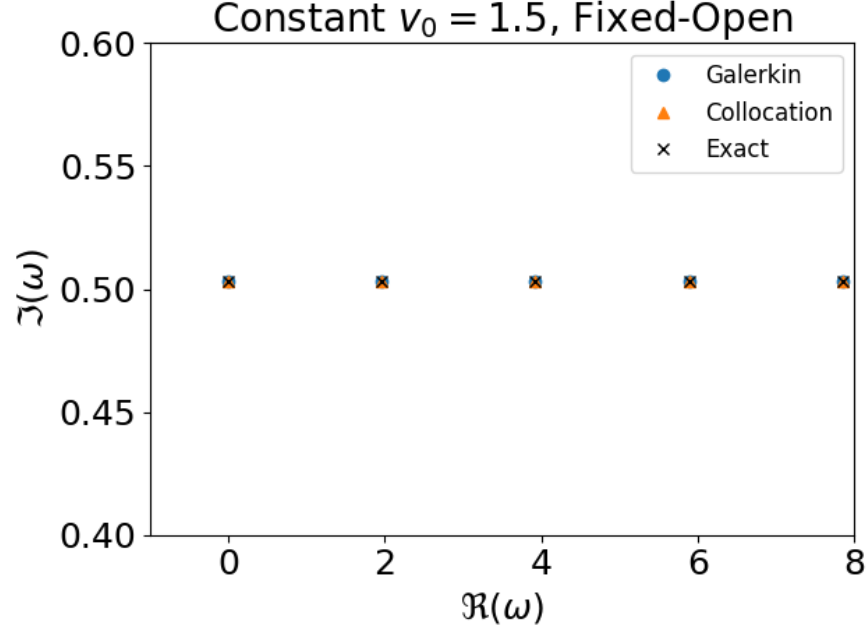
Figure 3.11: Showing the first 5 filtered eigenmodes of each method. They are unstable. The spectral methods agree with theoretical eigenvalues.

3.6 Plasma Flow with Spatial Varying Velocity Profiles

This section we will apply spectral methods to Eq. (2.38) with Dirichlet boundary and fixed-open boundary conditions. The parameters for spectral methods are the same as Table. 3.1.

3.6.1 Subsonic Case

No spurious modes found in subsonic case.

Dirichlet Boundary

When setting the mid-point velocity to be $M_m = 0.5$, we have the subsonic velocity profile. This velocity profile is the orange line shown in Fig. 2.4. With Dirichlet boundary condition, $\tilde{v}(\pm 1) = 0$. The flow in magnetic nozzle is stable. Fig. 3.12 shows the first few eigenvalues obtained by different discretizations.

The order of growth rates obtained by different methods is 10^{-13}, we can consider it to be stable.
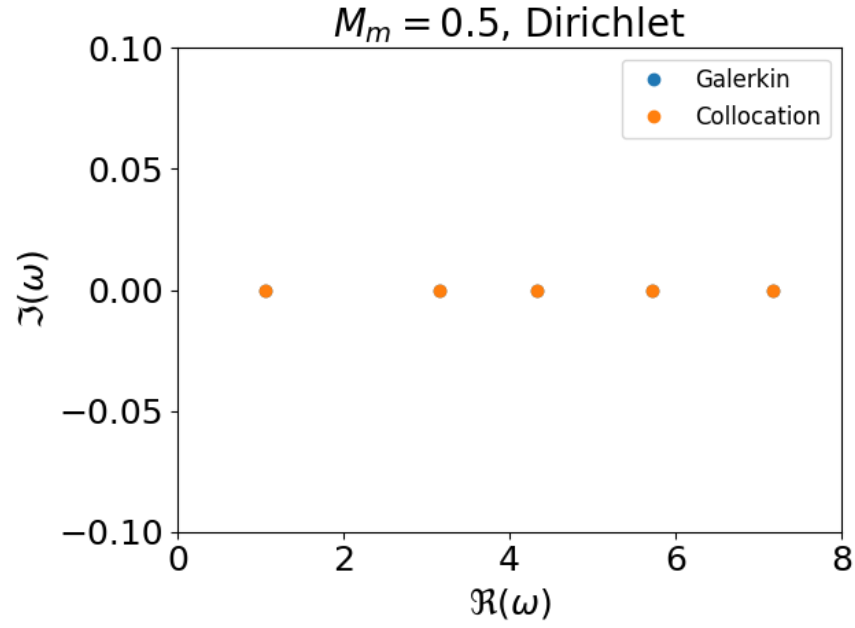
Figure 3.12: Showing the first 5 modes. They are stable. Two methods agree with each other.

Fixed-Open Boundary
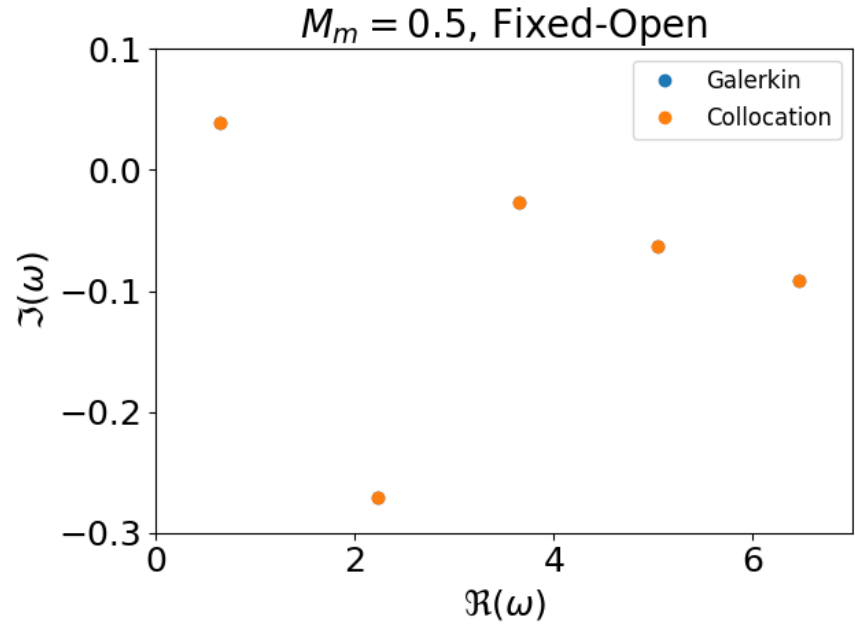
Figure 3.13: Showing the first 5 modes. The ground mode is unstable, other modes are stable.

3.6.2 Supersonic Case

In the supersonic case, spurious modes occur and we need to apply convergence test to extract true eigenvalues.

Dirichlet Boundary

When the velocity profile is supersonic, shown as purple line in Fig. 2.4, spurious modes appeared as predicted in Sec. 3.4.1. Using the convergence test, we successfully eliminated all spurious modes. Fig. 3.14 shows the first few filtered eigenvalues. As we can see the flow is stable.
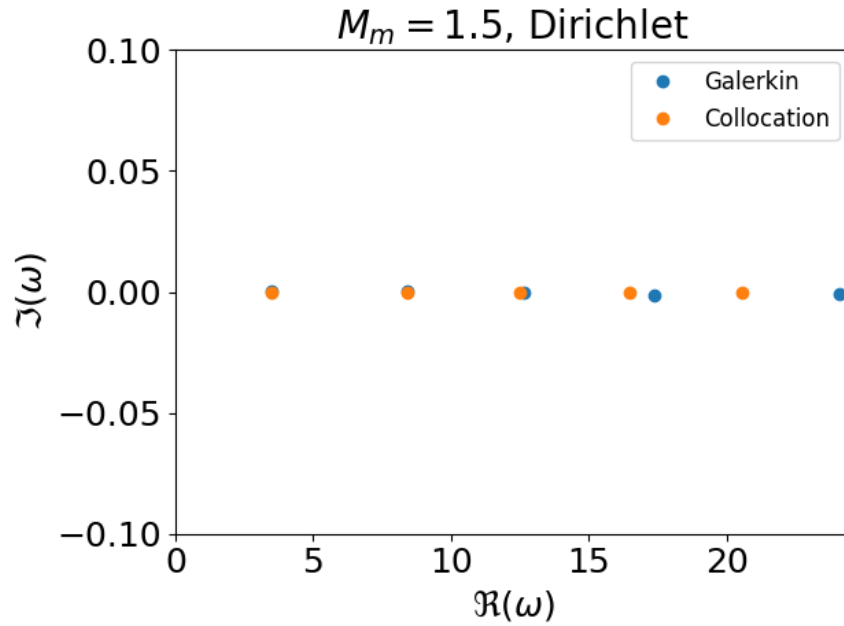
Figure 3.14: First 5 eigenmodes are shown, they are stable. Two methods agree well on the first 3 eigenmodes, and starts to deviate from each other after that.

Fixed-Open Boundary

All modes are unstable.
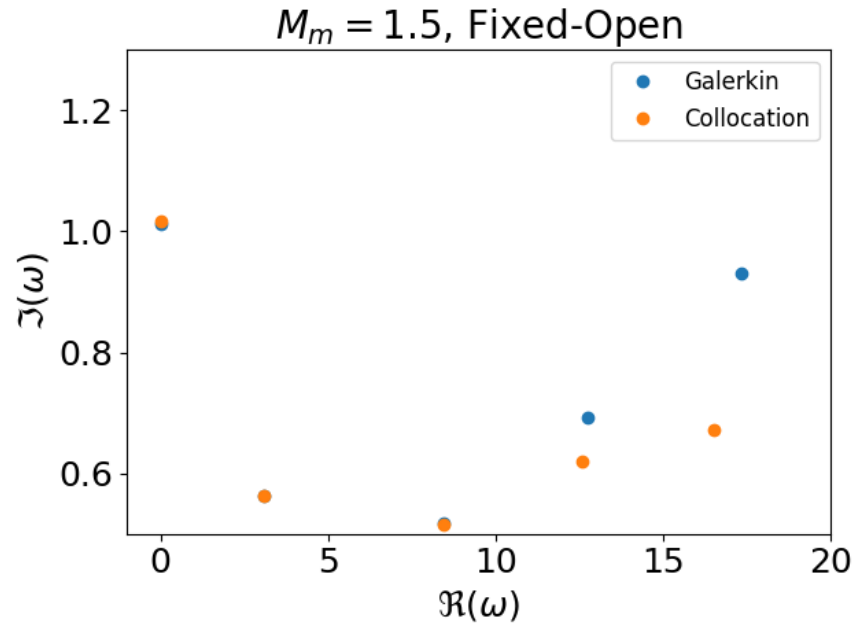
Figure 3.15: Showing the first 5 filtered eigenmodes, they are unstable. Two methods agree well on the first 3 modes, and start to have significant difference after that.

Chapter 4

Singular Perturbation

When dealing with the accelerating velocity profile, spectral methods struggle to yield meaningful results because of the singularity at the nozzle throat ($z = 0$). This chapter is dedicated to analyze the polynomial eigenvalue problem with transonic velocity profile. We start by showing the existence of the singularity of Eq. (2.38), and how spectral methods introduced in previous chapter failed to resolve solutions. Then we will discuss the concept of singular perturbation and will pickup regular solutions to Eq. (2.38) near the nozzle throat $z = 0$ using Frobenius method. Finally, we will introduce shooting method and use it together with the regular solutions to find eigenmodes.

4.1   Presence of Singularity in Transonic cases

In order to see the existence of the singularity, we rearrange the terms the polynomial eigenvalue problem, Eq. (2.38),

$$
\begin{aligned}
&(1 - v_0^2)\frac{\partial^2 \tilde{v}}{\partial z^2} \\
&+ \left[2i\omega v_0 - \left(3v_0 + \frac{1}{v_0} \right) \frac{\partial v_0}{\partial z} \right] \frac{\partial \tilde{v}}{\partial z} \\
&+ \left[\omega^2 + 2i\omega \frac{\partial v_0}{\partial z} - \left(1 - \frac{1}{v_0^2} \right) \left(\frac{\partial v_0}{\partial z} \right)^2 - \left(v_0 + \frac{1}{v_0} \right) \frac{\partial^2 v_0}{\partial z^2} \right] \tilde{v} \\
&= 0
\end{aligned}
\tag{4.1}
$$

This is a second order ordinary differential equation defined on region $[-1, 1]$.

For transonic (accelerating and decelerating) velocity profiles (Fig. 2.4), the plasma flow is at sonic point at the throat of the nozzle, $v_0(0) = 1$. Therefore, the highest order term vanishes at $z = 0$. It is a singular point, and it is the cause of the failure of spectral

method, see Fig. (4.1). Spectral method is unable to resolve meaningful eigenfunctions, the eigenfunctions are squeezed together at $z = 0$, hence resulting wrong eigenvalues.
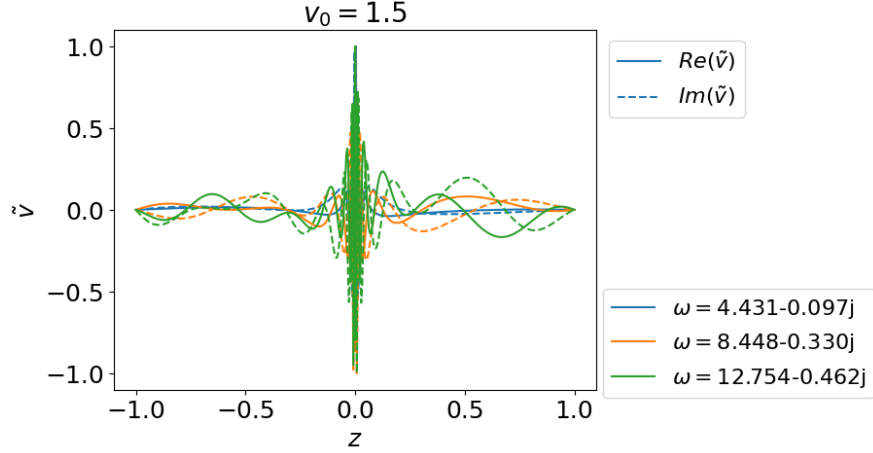
Figure 4.1: An attempt to solve the polynomial eigenvalue problem, Eq. (2.38) using finite-difference. Eigenfunctions are squeezed to the center of the nozzle due to the existence of the singularity at $z = 0$.

4.2 Expansion at Singularity

In this section, we will try to extract the regular solutions to Eq. (4.1) using Frobenius method. It is speculated such regular solutions exist. Further analysis and numerical simulations also validate the existence of such solutions. In order to find them, we need to expand terms in Eq. (4.1) about the singularity.

The first task is to linearize the terms with v_0 about the singularity. The linearization of $v_0(z) = 1 + v_0'(0)z$ is a good approximation to the original function $v_0(z)$ because the transonic velocity profiles are linear in the neighborhood of $z = 0$, as we can see from Fig. 2.4. Therefore, through some simple algebra we obtain,

$$
\begin{aligned}
1 - v_0^2 &= -2v_0'(0)z \\
3v_0 + \frac{1}{v_0} &= 4 + 2v_0'(0)z \\
1 - \frac{1}{v_0^2} &= 2v_0'(0)z \\
v_0 + \frac{1}{v_0} &= 2
\end{aligned}
$$

$$(4.2)$$

Then Eq. (4.1) becomes

$$-2v_0'(0)z\frac{\partial^2 \tilde{v}}{\partial z^2}$$

$$+[2i\omega - 4v_0'(0) + (2i\omega - 2v_0'(0))z]\frac{\partial \tilde{v}}{\partial z} \tag{4.3}$$

$$+\left[\omega^2 + 2i\omega v_0'(0) - 2v_0''(0) - 2v_0'(0)^3 z\right]\tilde{v} = 0$$

In fact, we can further simply the equation by dropping all z terms except the first term (second-order derivative term). It can be shown that dropping the z terms except the second derivative in Eq. (4.3) does not affect the first order correction ($\tilde{v}$ is the same up to z term), it is an acceptable approximation.

$$-2v_0'(0)z\frac{\partial^2 \tilde{v}}{\partial z^2} + (2i\omega - 4v_0'(0))\frac{\partial \tilde{v}}{\partial z} + (\omega^2 + 2i\omega v_0'(0) - 2v_0''(0))\tilde{v} = 0 \tag{4.4}$$

Dividing by the first coefficient, we have

$$z\frac{\partial^2 \tilde{v}}{\partial z^2} + a\frac{\partial \tilde{v}}{\partial z} + b\tilde{v} = 0 \tag{4.5}$$

where
$$a = \frac{2i\omega - 4v_0'(0)}{-2v_0'(0)}; \quad b = \frac{\omega^2 + 2i\omega v_0'(0) - 2v_0''(0)}{-2v_0'(0)} \tag{4.6}$$

Use Frobenius method, we assume the velocity perturbation can be written as a power series in z, $\tilde{v} = \sum_{n\geq 0} c_n z^{n+r}$. By substituting the power series into Eq. (4.5) we have

$$\sum_{n\geq 0}(n+r)(n+r+1)c_n z^{n+r-1} + a(n+r)c_n z^{n+r-1} + bc_n z^{n+r} = 0 \tag{4.7}$$

Shift the power of the last term we get

$$\sum_{n\geq 0}(n+r)(n+r+1)c_n z^{n+r-1} + a(n+r)c_n z^{n+r-1} + \sum_{n\geq 1}bc_{n-1}z^{n+r-1} = 0 \tag{4.8}$$

Setting $n = 0$, we get the indicial equation

$$c_0 r(r-1) + c_0 ar = 0 \Rightarrow c_0 r(r+a-1) = 0 \tag{4.9}$$

We get two different roots, $r = 0$ and $r = 1 - a$. They correspond to finite solution and diverging solution near the singularity, respectively.

The coefficients are given by recurrence relation

$$(n+r)(n+r-1)c_n + a(n+r)c_n + bc_{n-1} = 0 \Rightarrow c_n = \frac{-bc_{n-1}}{(n+r)(n+r-1+a)} \tag{4.10}$$

Solving this relation we get explicit expression for c_n, $n \in \mathbb{N}$,

$$
\begin{aligned}
c_n &= \frac{(-1)^n b^n c_0}{\prod_{k=0}^{n-1}(n+r-k)(n+r-1+a-k)} \\
&= (-1)^n b^n c_0 \frac{\Gamma(r+1)\Gamma(r+a)}{\Gamma(n+r+1)\Gamma(n+r+a)}
\end{aligned}
\tag{4.11}
$$

Therefore, we successfully extracted the regular solution (corresponding to the root $r = 0$) in the form of power series,

$$
\begin{aligned}
\tilde{v} &= c_0 + c_1 z + c_2 z^2 + \cdots \\
&= c_0 - c_0 \frac{b}{a} z + c_0 \frac{b^2}{2a(1+a)} z^2 + \cdots
\end{aligned}
\tag{4.12}
$$

It is worth to mention that the diverging solution (corresponding to the root $r = a$) goes like

$$\tilde{v}(z) \sim z^{1-a} = z^{-1-\omega_i/v_0'(0)} z^{i\omega_r/v_0'(0)} \tag{4.13}$$

where $\omega = \omega_r + i\omega_i$. Meaning that the divergent solution will start to diverge when $\omega_i > -v'(0)$.

4.3   Shooting Method

The existence of divergent solutions makes the problem hard to solve numerically using spectral method. One workaround involves manually selecting regular solutions during the numerical process. The shooting method, a suitable numerical technique, is capable of incorporating information of regular solutions. In other words, $\tilde{v}$ and its derivatives at the nozzle throat $z = 0$ can be incorporate into the numerical process. Due to this restriction of singularity, we are not allowed to impose any boundary condition at the nozzle exit, $z = 1$, anymore because the information of the regular solution already serve as a boundary condition.

Our polynomial eigenvalue problem, Eq. (2.38), can be formulated in the following form,

$$f(z, \tilde{v}, \tilde{v}', \tilde{v}''; \omega) = 0 \quad -1 \le z \le 0, \quad \tilde{v}(-1) = 0, \tilde{v}(0) = 1 \tag{4.14}$$

where f is the function defined on the left of equal sign of Eq. (2.38). The task for shooting

method is to find eigenvalues ω and their corresponding eigenfunctions $\tilde{v}$ such that $f = 0$ holds. Meanwhile, the eigenfunctions must satisfy the boundary conditions at the entrance $z = -1$ and at the throat $z = 0$. After obtaining the solutions, we can extend the solution to $z = 1$. The extension is unique, more details will be explained later.

However, to make the formulation more suitable for numerical computation, we would like to rewrite the second differential equation as two first order differential equations,

$$\frac{\mathrm{d}}{\mathrm{d}z}\tilde{\mathbf{u}} = \mathbf{f}(\tilde{\mathbf{u}}, z; \omega), \quad -1 \le z \le 0, \quad \tilde{v}(-1) = 0, \tilde{v}(0) = 1 \tag{4.15}$$

Let $\tilde{\mathbf{u}} = [\tilde{v}, \tilde{u}]^T$, the polynomial eigenvalue problem is transformed to

$$\tilde{v}' = \tilde{u}$$
$$\tilde{u}' = \frac{-1}{1 - v_0^2}\left[\omega^2\tilde{v} + 2i\omega(v_0 + v_0'\tilde{v}) - \left(3v_0 - \frac{1}{v_0}\right)v_0'\tilde{u} - \left(1 - \frac{1}{v_0}^2\right)(v_0')^2\tilde{v} - \left(v_0 + \frac{1}{v_0}v_0''\tilde{v}\right)\right]$$

together with two boundary conditions, $\tilde{v}(-1) = 0$ and $\tilde{v}(0) = 1$. The task of shooting method remains the same: find $\tilde{\mathbf{u}}$ and ω such that $\mathrm{d}\tilde{\mathbf{u}}/\mathrm{d}z = \mathbf{f}$ and $\tilde{v}$ must satisfy the boundary conditions.

Suppose ω is given. We can find $\tilde{\mathbf{u}}(-1)$, and hence $\tilde{v}(-1)$ by applying 4th order Runge-Kutta method (RK4) to the following IVP,

$$\frac{\mathrm{d}}{\mathrm{d}z}\tilde{\mathbf{u}} = \mathbf{f}(\tilde{\mathbf{u}}, z; \omega), \quad -1 \le z \le 0, \quad \tilde{\mathbf{u}}(0) = \begin{bmatrix} \tilde{v}(0) \\ \tilde{u}(0) \end{bmatrix}, \frac{\mathrm{d}}{\mathrm{d}z}\tilde{\mathbf{u}}(0) = \begin{bmatrix} \tilde{v}'(0) \\ \tilde{u}'(0) \end{bmatrix} \tag{4.16}$$

The information of the regular solution is built into the numerical process by setting the initial conditions,

$$\tilde{\mathbf{u}} = \begin{bmatrix} \tilde{v}(0) \\ \tilde{u}(0) \end{bmatrix} = \begin{bmatrix} c_0 \\ c_1 \end{bmatrix} = \begin{bmatrix} 1 \\ (2i\omega v_0' - 2v_0'')/2v_0' \end{bmatrix}$$
$$\frac{\mathrm{d}}{\mathrm{d}z}\tilde{\mathbf{u}} = \begin{bmatrix} \tilde{v}'(0) \\ \tilde{u}'(0) \end{bmatrix} = \begin{bmatrix} \tilde{u}(0) \\ c_2 \end{bmatrix} = \begin{bmatrix} (2i\omega v_0' - 2v_0'')/2v_0' \\ -((v_0')^4 + (2i\omega v_0' + (v_0')^2 - v_0'')(i\omega v_0' - v_0''))/(v_0'(2i\omega - 6v_0')) \end{bmatrix} \tag{4.17}$$

The coefficients c_0, c_1, and c_2 are obtained from the power series expansion of $\tilde{v}$ near $z = 0$, Eq. (4.12).

The above step can be abstracted as a function, $h(\omega) = \tilde{v}(-1)$. This function takes in a variable ω, and it spits out the value $\tilde{v}(-1)$ by applying RK4 to the I.V.P. Eq. (4.16).

We then apply root finding algorithm to this function h to find ω such that $\tilde{v}$ satisfies the boundary condition at the entrance, $h(\omega) = \tilde{v}(-1) = 0$. This process can be viewed as trying to land a projectile at certain location, i.e. $\tilde{v}(-1) = 0$, by adjusting the shooting angle, i.e. ω, hence the name shooting method.

After finding ω, we can extend the numerical solution $\tilde{v}$ to the region $[0, 1]$. We simply apply RK4 to the following I.V.P.

$$\frac{\mathrm{d}}{\mathrm{d}z}\tilde{\mathbf{u}} = \mathbf{f}(\tilde{\mathbf{u}}, z; \omega), \quad 0 \le z \le 1, \quad \tilde{\mathbf{u}}(0) = \begin{bmatrix} \tilde{v}(0) \\ \tilde{u}(0) \end{bmatrix}, \frac{\mathrm{d}}{\mathrm{d}z}\tilde{\mathbf{u}}(0) = \begin{bmatrix} \tilde{v}'(0) \\ \tilde{u}'(0) \end{bmatrix} \tag{4.18}$$

Since ω is already found, the initial conditions are given. The function $\mathbf{f}$ is continuous in z on $[0, 1]$ and is Lipschitz in $\tilde{\mathbf{u}}$ due to the fact $\mathbf{f}$ is continuous on a compact region $[0, 1]$. Hence, the solution to this I.V.P. exists and is unique.

4.4   Plasma Flow with Accelerating Velocity Profile

Starting from the singular point, we shoot the regular solution to the left boundary. We find the set of eigenvalues such that $\tilde{v}(-1) = 0$. With these eigenvalues, we can extend the solution to the supersonic region $(0, 1]$. The first few eigenmodes are drawn in Fig. 4.2. The eigenmodes indicates that the accelerating plasma flow is stable.
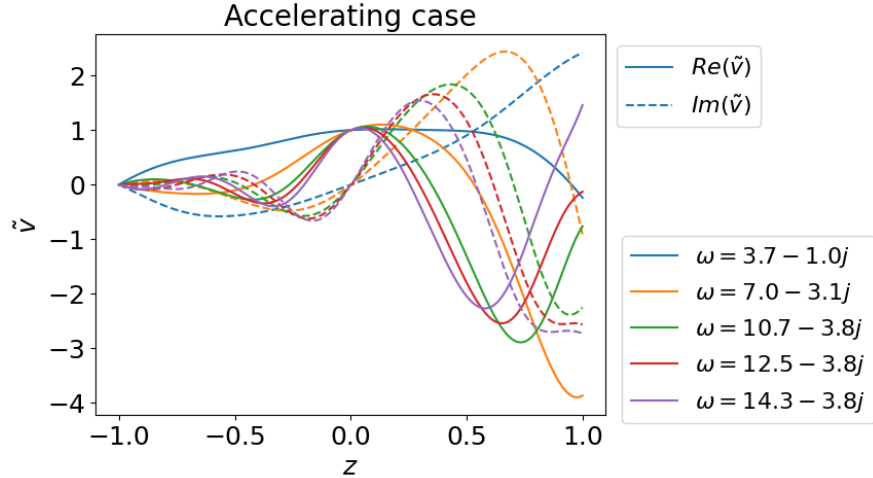
Figure 4.2: Showing the first 5 eigenmodes, they are stable.

Chapter 5

Discussion

5.1 Summary of the Results

For the subsonic flow, it is stable under Dirichlet boundary condition. It is also stable under fixed-open boundary, except for ground mode when velocity is nonuniform. For the supersonic flow, it is stable when Dirichlet boundary condition is applied, and unstable is the boundary condition is fixed-open. The results are summarized in Table. 5.1.

The flow with accelerating velocity profile is stable, assuming there is no velocity perturbation at the entrance of the nozzle. On the other hand, the decelerating flow is physically impossible under the boundary condition where velocity perturbation is 0 at the entrance. The results are summarized in Table. 5.2.

Table 5.1: The Dirichlet boundary condition means there are no perturbations at the two ends of the nozzle. While the fixed-open condition assume that there is no perturbation at the entrance of the nozzle, $\tilde{v}(-1) = 0$, and then the derivative with respect to z of the velocity perturbation is 0 at the exit, $\partial_z \tilde{v}(1) = 0$.

	Subsonic	Supersonic
Dirichlet	Stable	Stable
Fixed-Open	Stable (except ground mode for variable velocity profile)	Unstable

Table 5.2: The boundary condition is set so that there is no perturbation at the entrance of the nozzle, $\tilde{v}(-1) = 0$, and then reaches a finite value at the throat of the nozzle, $\tilde{v}(0) = 1$.

Accelerating	Decelerating
Stable	Impossible

5.2 Limitations of the methods

5.2.1 Spectral Method

The spectral method suffers the spectral pollution. For now there is no automatic ways to filter spurious modes other than doing convergence test and pick up the convergent eigenvalues manually by ourselves. We believe there is a discretization scheme that is spectral pollution free. We made such optimistic guess based on the following example. Let's transform Eq. 2.39 with Dirichlet boundary condition $\tilde{v}(\pm 1) = 0$ to its normal form, that is

$$u''(z) + r(z)u(z) = 0, \quad u(\pm 1) = 0 \tag{5.1}$$

by doing the change of variables

$$u(z) = \exp\left(\frac{iv_0\omega}{1 - v_0^2}\right)\tilde{v}(z); \quad r(z) = \frac{\omega^2}{(1 - v_0^2)^2} \tag{5.2}$$

This scheme is spectral pollution free. Meaning that no spurious modes will occur if we apply spectral methods to this transformed problem.

5.2.2 Shooting Method

The shooting method is not exhaustive due to the nature of root finding algorithm. A root can only be found if the initial guess of the root is close enough to the actual root. To work around this issue, we have to perform a grid search on the complex plane. This way we can only survey the low frequency region due to finite computing resources. The conclusion for cases with transonic velocity profiles is true only for low frequency region.

5.3 Conclusion

In Chap. 2, we derived the linearized equations of motion of the flow in one dimensional magnetic nozzle. Furthermore, we rewrite the linearized governing equations as an eigenvalue problem. Using the spectral methods introduced in chapter 2, we discretized the operators of the problem. Hence, transforming it into an algebraic eigenvalue problem.

With the aid of computer, we are able to solve the algebraic eigenvalue problem. The results show that the flow in magnetic nozzle with Dirichlet boundary condition is stable except the case with decelerating velocity profile.

Bibliography

[1] Cpep - contemporary physics education project. Accessed: March 26, 2024.

[2] Shair. author Ahmad. *A Textbook on Ordinary Differential Equations*. UNITEXT, 88. Second edition. edition.

[3] Toshiki Aikawa. The stability of spherically symmetric accretion flows. *Astrophys Space Sci*, 66(2):277–285, December 1979.

[4] S. A. Andersen. Continuous Supersonic Plasma Wind Tunnel. *Phys. Fluids*, 12(3):557, 1969.

[5] H. Bondi. On Spherically Symmetrical Accretion. *Monthly Notices of the Royal Astronomical Society*, 112(2):195–204, April 1952.

[6] R. W. Boswell, O. Sutherland, C. Charles, J. P. Squire, F. R. Chang Díaz, T. W. Glover, V. T. Jacobson, D. G. Chavers, R. D. Bengtson, E. A. Bering, R. H. Goulding, and M. Light. Experimental evidence of parametric decay processes in the variable specific impulse magnetoplasma rocket (VASIMR) helicon plasma source. *Physics of Plasmas*, 11(11):5125–5129, November 2004.

[7] Lyonell Boulton. Spectral pollution and eigenvalue bounds. *Applied Numerical Mathematics*, 99:1–23, January 2016.

[8] Richard L Burden, J Douglas Faires, and Annette M Burden. *Numerical Analysis*. 2016.

[9] Francis F. Chen. *Introduction to Plasma Physics and Controlled Fusion*. Springer International Publishing, Cham, 2016.

[10] Steven R. Cranmer. New views of the solar wind with the Lambert W function. *American Journal of Physics*, 72(11):1397–1403, November 2004.

[11] Roldão da Rocha. Black hole acoustics in the minimal geometric deformation of a de Laval nozzle. *The European Physical Journal C*, 77(5):355, 5 2017. [Online; accessed 2023-03-02].

[12] L. Del Zanna, M. Velli, and P. Londrillo. Dynamical response of a stellar atmosphere to pressure perturbations: numerical simulations.

[13] Hironobu Furuhashi, Yasusada Nambu, and Hiromi Saida. Simulation of an acoustic black hole in a Laval nozzle. *Class. Quantum Grav.*, 23(17):5417–5438, September 2006.

[14] J. Gaite. Perturbations in the self-similar Bondi flow. 449(3):861–868.

[15] R. Grappin, E. Cavillier, and M. Velli. Acoustic waves in isothermal winds in the vicinity of the sonic point.

[16] Seung-Yeal Ha, Taeyoung Ha, Chi-Ok Hwang, and Ho Lee. Nonlinear instability of the one-dimensional Vlasov-Yukawa system. *Journal of Mathematical Physics*, 52(3):033301, March 2011.

[17] Klaus Jockers. On the stability of the solar wind. *Sol Phys*, 3(4):603–610, April 1968.

[18] Igor D. Kaganovich, Andrei Smolyakov, Yevgeny Raitses, Eduardo Ahedo, Ioannis G. Mikellides, Benjamin Jorns, Francesco Taccogna, Renaud Gueroult, Sedina Tsikata, Anne Bourdon, Jean-Pierre Boeuf, Michael Keidar, Andrew Tasman Powis, Mario Merino, Mark Cappelli, Kentaro Hara, Johan A. Carlsson, Nathaniel J. Fisch, Pascal Chabert, Irina Schweigert, Trevor Lafleur, Konstantin Matyash, Alexander V. Khrabrov, Rod W. Boswell, and Amnon Fruchtman. Physics of E × B discharges relevant to plasma propulsion and similar technologies. *Physics of Plasmas*, 27(12):120601, 12 2020.

[19] Eric Keto. Stability and solution of the time-dependent Bondi–Parker flow. *Monthly Notices of the Royal Astronomical Society*, 493(2):2834–2840, April 2020.

[20] R. Kolman, M. Okrouhlík, A. Berezovski, D. Gabriel, J. Kopačka, and J. Plešek. B-spline based finite element method in one-dimensional discontinuous elastic wave propagation. *Applied Mathematical Modelling*, 46:382–395, June 2017.

[21] O. Koshkarov, A. I. Smolyakov, I. D. Kaganovich, and V. I. Ilgisonis. Ion sound instability driven by the ion flows. *Phys. Plasmas*, 22(5):052113, May 2015.

[22] Erwin Kreyszig. *Introductory functional analysis with applications*. Wiley, New York, 1978.

[23] Justin M Little. Performance scaling of magnetic nozzles for electric propulsion, 2015. ISBN: 9781321565317.

[24] Andrei A. Litvak and Nathaniel J. Fisch. Rayleigh instability in Hall thrusters. *Physics of Plasmas*, 11(4):1379–1383, April 2004.

[25] X. Llobet, K. Appert, A. Bondeson, and J. Vaclavik. On spectral pollution. *Computer Physics Communications*, 59(2):199–216, June 1990.

[26] Stéphane Mazouffre. Electric propulsion for satellites and spacecraft: established technologies and novel approaches. *Plasma Sources Sci. Technol.*, 25(3):033002, June 2016.

[27] Satoshi Okuzumi and Masa-aki Sakagami. Quasinormal ringing of acoustic black holes in Laval nozzles: Numerical simulations.

[28] Ivan Romadanov, Andrei Smolyakov, Yevgeny Raitses, Igor Kaganovich, Tang Tian, and Sergei Ryzhkov. Structure of nonlocal gradient-drift instabilities in Hall E × B discharges. *Physics of Plasmas*, 23(12):122111, December 2016.

[29] D. D. Ryutov, P. N. Yushmanov, D. C. Barnes, and S. V. Putvinski. Divertor for a linear fusion device. page 060003, Newport Beach, CA, USA, 2016.

[30] Jie Shen, Tao Tang, and Li-Lian Wang. *Spectral Methods.* Springer Berlin Heidelberg.

[31] A. I. Smolyakov, A. Sabo, P. Yushmanov, and S. Putvinskii. On quasineutral plasma flow in the magnetic nozzle. *Physics of Plasmas*, 28(6):060701, June 2021.

[32] R. F. Stellingwerf and J. Buff. Stability of astrophysical gas flow. I - Isothermal accretion. *ApJ*, 221:661, April 1978.

[33] T. Theuns and M. David. Spherically symmetric, polytropic flow. 384:587.

[34] Satoshi Togo, Tomonori Takizuka, Dirk Reiser, Mizuki Sakamoto, Yuichi Ogawa, Naomichi Ezumi, Kenzo Ibano, Kunpei Nojiri, Yue Li, and Yousuke Nakashima. Characteristics of plasma flow profiles in a super-X-divertor-like configuration. *Nuclear Materials and Energy*, 19:149–154, May 2019.

[35] Lloyd N. (Lloyd Nicholas) Trefethen. *Spectral methods in MATLAB.* Software, environments, tools. Society for Industrial and Applied Mathematics, Philadelphia, PA, 2000.

[36] WG Unruh. Sonic analogue of black holes and the effects of high frequencies on black hole evaporation. *Physical review. D, Particles and fields*, 51(6):2827–2838, 1995.

[37] M. Velli. From supersonic winds to accretion: Comments on the stability of stellar winds and related flows. 432:L55.

[38] M. Velli. Hydrodynamics of the Solar Wind Expansion. 277(1/2):157–167.

[39] Craig H. Williams. Fusion Propulsion Through a Magnetic Nozzle and Open Divertor. In *AIP Conference Proceedings*, volume 654, pages 510–515, Albuquerque, New Mexico (USA), 2003. AIP. ISSN: 0094243X.

Appendix A

Verification of Analytical Solutions

The general solution to

$$\omega^2 \tilde{v} + 2i\omega \frac{\partial \tilde{v}}{\partial z} + (1 - v_0^2)\frac{\partial^2 \tilde{v}}{\partial z^2} = 0$$

is

$$\tilde{v} = \exp\left(-\frac{i\omega}{v_0 + 1}\right)\left[\exp\left(i\omega\frac{z+1}{v_0+1}\right) - \exp\left(i\omega\frac{z+1}{v_0-1}\right)\right]$$

To show this, we first find the derivatives of $\tilde{v}$,

$$\tilde{v} = \exp\left(-\frac{i\omega}{v_0 + 1}\right)\left[\exp\left(i\omega\frac{z+1}{v_0+1}\right) - \exp\left(i\omega\frac{z+1}{v_0-1}\right)\right]$$

$$\frac{\partial \tilde{v}}{\partial z} = i\omega \exp\left(-\frac{i\omega}{v_0 + 1}\right)\left[\frac{1}{v_0+1}\exp\left(i\omega\frac{z+1}{v_0+1}\right) - \frac{1}{v_0-1}\exp\left(i\omega\frac{z+1}{v_0-1}\right)\right]$$

$$\frac{\partial^2 \tilde{v}}{\partial z^2} = -\omega^2 \exp\left(-\frac{i\omega}{v_0 + 1}\right)\left[\frac{1}{(v_0+1)^2}\exp\left(i\omega\frac{z+1}{v_0+1}\right) - \frac{1}{(v_0-1)^2}\exp\left(i\omega\frac{z+1}{v_0-1}\right)\right]$$

Then the rest is easy,

$$\omega^2 \tilde{v} + 2i\omega \frac{\partial \tilde{v}}{\partial z} + (1 - v_0^2)\frac{\partial^2 \tilde{v}}{\partial z^2}$$

$$= \exp\left(-\frac{i\omega}{v_0 + 1}\right)\left(1 - \frac{2v_0}{v_0+1} + \frac{(1-v_0^2)}{(v_0+1)^2}\right)\exp\left(i\omega\frac{z+1}{v_0+1}\right)$$

$$- \exp\left(-\frac{i\omega}{v_0 + 1}\right)\left(1 - \frac{2v_0}{v_0-1} + \frac{(1-v_0^2)}{(v_0-1)^2}\right)\exp\left(i\omega\frac{z+1}{v_0-1}\right)$$

$$= 0$$

If $\omega = n\pi(1 - v_0^2)/2$, then $\tilde{v}(\pm 1) = 0$. It is easy to see that $v(-1) = 0$. As for $z = 1$, we

have

$$\tilde{v}(1) \propto \exp\left(\frac{2i\omega}{v_0 + 1}\right) - \exp\left(\frac{2i\omega}{v_0 - 1}\right)$$

$$= \exp(in\pi(1 - v_0)) - \exp(-in\pi(1 + v_0))$$

$$= (-1)^n \exp(-in\pi v_0) - (-1)^n \exp(-in\pi v_0)$$

$$= 0$$

If

$$\omega = (v_0^2 - 1)\left[\frac{n\pi}{2} - \frac{1}{4}i\ln\left(\frac{v_0 - 1}{v_0 + 1}\right)\right]$$

then $\tilde{v}(-1) = 0$ and $\partial_z\tilde{v}(1) = 0$. It is easy to see that $v(-1) = 0$. The derivative at $z = 1$ is

$$\left.\frac{\partial\tilde{v}}{\partial z}\right|_{z=1} \propto \frac{1}{v_0 + 1}\exp\left(\frac{2i\omega}{v_0 + 1}\right) - \frac{1}{v_0 - 1}\exp\left(\frac{2i\omega}{v_0 - 1}\right)$$

$$= \frac{1}{v_0 + 1}\exp\left(in\pi(v_0 - 1) + \frac{v_0 - 1}{2}\ln\left(\frac{v_0 - 1}{v_0 + 1}\right)\right)$$

$$- \frac{1}{v_0 - 1}\exp\left(in\pi(v_0 + 1) + \frac{v_0 + 1}{2}\ln\left(\frac{v_0 - 1}{v_0 + 1}\right)\right)$$

$$= \frac{(-1)^n}{v_0 + 1}\exp(in\pi v_0)\left(\frac{v_0 - 1}{v_0 + 1}\right)^{(v_0-1)/2}$$

$$- \frac{(-1)^n}{v_0 - 1}\exp(in\pi v_0)\left(\frac{v_0 - 1}{v_0 + 1}\right)^{(v_0+1)/2}$$

$$= 0$$

The last equality holds because

$$\frac{1}{v_0 - 1}\left(\frac{v_0 - 1}{v_0 + 1}\right)^{(v_0+1)/2} = \frac{1}{v_0 + 1}\left(\frac{v_0 - 1}{v_0 + 1}\right)^{(v_0-1)/2}$$